# Determination of Manning's Roughness Coefficient and Chezy's Coefficient for Different Bed Materials

*A Thesis Submitted in Fulfillment of the Requirement for the Award of the Degree of*

MASTER OF ENGINEERING

in Civil Infrastructure

Submitted By

AASHREY GOEL

801523001

Under Supervision of

Dr. B.S Das
(Assistant Professor)

Dr. Richa Babbar
(Assistant Professor)


DEPARTMENT OF CIVIL ENGINEERING

THAPAR INSTITUTE OF ENGINEERING & TECHNOLOGY (A DEEMED TO BE UNIVERSITY), PATIALA, PUNJAB

## CERTIFICATE

This is to certify that the theis entitled "Determination of Manning's Roughness Coefficient and Chezy's Coefficient for different bed materials" is a bonafide record of the work carried out by me for the fulfillment of requirements for the award of degree of Master of Engineering in Civil Infrastructure from Thapar Institute of engineering and technology, Patiala under the guidance and supervision of Dr. B.S Das (Assistant Professor, Civil engineering Department) and Dr. Richa Babbar (Assistant Professor, Civil engineering Department) during January, 2017 to December, 2018.

Date: 19-04-2019

Aashrey Goel
(801523001)

It is certified that the above statement made by the student is true to the best of our knowledge.

Dr. Richa Babbar
(Assistant Professor)
Department of Civil Engineering
Thapar Institute of Engineering
and technology, Patiala

Dr. Bhabani Shankar Das
(Assistant Professor)
Department of Civil Engineering
Thapar Institute of Engineering
and technology, Patiala

## DECLARATION

I, Aashrey Goel, hereby declare that the work presented in this thesis entitled "Determination of Manning's Roughness Coefficient and Chezy's Coefficient for Different Bed Materials" in fulfillment of the requirement for the award of degree of Master of Engineering (Civil Infrastructure) submitted at Department of Civil Engineering , Thapar Institute of Engineering & Technology (Deemed to be University), Patiala is an authentic record of work carried out under supervision of Dr. Richa Babbar ( Department of Civil Engineering, Thapar Instutute of Engineering and technology) and Dr. Bhabani Shankar Das ( Department of Civil Engineering, Thapar Instutute of Engineering and technology) from January, 2017 to October, 2018. The matter presented in this has not been submitted either in part or full to any other university or institute for the award of any other degree.

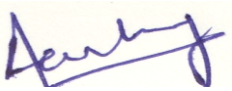

Date: 19-04-2019

(Aashrey Goel)
(801523001)

## ACKNOWLEDGEMENT

Firstly, I would like to express my heartly and sincere gratitude towards my supervisers Dr. B.S Das and Dr. Richa Babbar for guiding me throughout the project work. This work couldn't have come to completion without their invaluable guidance.

I would also like to thank Dr. Prem Pal Bansal, HOD, Department of civil engineering, for being supportive and giving me enough time to complete my work.

I want to thank the staff of Water Resources lab at Thapar University, Patiala for helping me with the experimental work and setup.

Lastly, I would thank God and my family for the unending strength and motivation they provided me with.

**Aashrey Goel**

## ABSTRACT

The present study is aimed at investigating the effect of bed roughness on various hydraulic flow parameters. The study primarily revolves around determination of Manning's roughness co-efficient (*n)* and Chezy's co-efficient (*C*) for three different conditions of bed roughness. Bed roughness was simulated and changed using two different materials as the bed form, i.e. sunboard and plastic fibre mat.

The experimental work has been performed in a re-circulating tilting flume. Three sections, 1 m apart are chosen as test sections and longitudinal velocity readings are recorded for whole flow depth at the centre of flume width. Two governing flow conditions are kept constant alternatively i.e., slope and discharge, and three runs of experimental investigations were carried out for each of these flow conditions.. All required geometrical and hydraulic parameters are calculated and thus, the values of roughness co-efficients *n* and *C* are determined. Velocity profiles have been plotted and the variations of velocity and other hydraulic parameters with the roughness co-efficients has been studied.

Velocity is found to increase with increase in discharge and slope for all the bed roughness conditions. Also, increase in roughness leads to increase in flow depth and a decrease in velocity. Plastic fibre mat has been found to have the highest value of *n* and the lowest value of *C* while sunboard being the smoothest of all bed forms boasts the lowest value of *n* and highest *C* value.

## TABLE OF CONTENTS


| Sr. No. | Name of the Chapters | Page No |
|---|---|---|
| | CERTIFICATE | i |
| | DECLARATION | ii |
| | ACKNOWLEDGEMENT | iii |
| | ABSTRACT | iv |
| | LIST OF TABLES | vii |
| | LIST OF FIGURES | viii |
| | GLOSSARY | xii |
| *Chapter 1* | Introduction | 1 |
| *1.1* | General | 1 |
| *1.2* | Classification of open channels | 2 |
| *1.3* | Types of open channel flows | 3 |
| *1.4* | Geometric elements of open channel flow | 5 |
| *1.5* | Geometric properties of different types of channels | 6 |
| *1.6* | Manning's equation for open channel flow | 8 |
| *1.7* | Chezy's co-efficient | 8 |
| *1.8* | Relevance of Manning's roughness co-efficient | 9 |
| *1.9* | Objectives | 9 |
| *1.10* | Organization of thesis | 9 |
| *Chapter 2* | Literature review | 11 |
| *2.1* | Open channel flow and hydraulic resistance | 11 |
| *2.2* | Critical review | 18 |
| *Chapter 3* | Experimental procedure and setup | 19 |
| *3.1* | General | 19 |
| *3.2* | Experimental setup | 19 |
| *3.3* | Experimental procedure | 22 |
| *3.4* | Used bed materials | 24 |
| *3.5* | Slope adjustment | 25 |
| *3.6* | Obtaining steady flow conditions in the flume | 25 |
| *Chapter 4* | Results and Discussions | 27 |

| | | |
|---|---|---|
| *4.1* | General | 27 |
| *4.2* | Variables and flow parameters | 27 |
| *4.3* | Vertical velocity profiles for different materials | 29 |
| *4.4* | Roughness co-efficients for different materials | 37 |
| *4.5* | Variation of Manning's '*n'* with velocity for different bed forms | 39 |
| *4.6* | Variation of Chezy's '*C*' with velocity for different bed forms | 40 |
| *4.7* | Variation of '*n'* and '*C'* with aspect ratio for different bed forms | 42 |
| *4.8* | Variation of Chezy's Coefficient (*C)* with Manning's Coefficient (*n)* | 45 |
| *4.9* | Roughness comparison between the various used bed materials | 46 |
| *Chapter 5* | Conclusions | 49 |
| | FUTURE SCOPE OF WORK | 51 |
| | REFERENCES | 52 |
| | DISSEMINATION OF WORK | 54 |

## LIST OF TABLES


| Sr. No. | Table details | Page No |
|---|---|---|
| Table 3.1 | Geometrical features of flume | 21 |
| Table 3.2 | Experimental runs and their characteristic flow parameters | 23 |
| Table 3.3 | Thickness of the used bed materials | 23 |
| Table 4.1 | Hydrological and Geometrical parameters for flow without any bed material. | 28 |
| Table 4.2 | Hydrological and Geometrical parameters for flow with sunboard as bed form. | 28 |
| Table 4.3 | Hydrological and Geometrical parameters for flow with Plastic fibre mat as the bed form. | 29 |
| Table 4.4 | Calculated values of *n* for no bed material | 37 |
| Table 4.5 | Calculated *n* values for sunboard as bed form | 38 |
| Table 4.6 | Calculated *n* values for plastic fibre mat as bed form. | 38 |

## LIST OF FIGURES


| Sr. No. | Table details | Page No |
|---|---|---|
| Figure 1.1 | Typical representation of an open channel-flow | 1 |
| Figure 1.2 | Open channel flow | 3 |
| Figure 1.3 | Diagrammatic representation of spatially-varied flow | 4 |
| Figure 1.4 | Geometric representation of open channel | 5 |
| Figure 1.5 | Cross-Section of a rectangular channel | 6 |
| Figure 1.6 | Cross-section of a trapezoidal channel | 6 |
| Figure 1.7 | Circular channel cross-section | 7 |
| Figure 1.8 | Triangular channel cross-section | 8 |
| Figure 3.1 | Tilting flume at Water Resources Lab, Thapar University, Patiala | 20 |
| Figure 3.2 | Schematic view of experimental setup | 20 |
| Figure 3.3 | Water supply motor | 21 |
| Figure 3.4 | Pitot Tube | 22 |
| Figure 3.5 | Sunboard used as a bed form | 24 |
| Figure 3.6 | Plastic fibre mat used as a bed form | 24 |
| Figure 3.7 | Hydraulic jack arrangement in the flume for changing slope. | 25 |
| Figure 4.1(a) | Vertical velocity profiles for no bed material at a constant slope of 0.004 and varying discharges at x = 3.15 m. | 30 |
| Figure 4.1(b) | Vertical velocity profiles for no bed material at a constant slope of 0.004 and varying discharges at x = 4.15 m. | 30 |
| Figure 4.1(c) | Vertical velocity profiles for no bed material at a constant slope of 0.004 and varying discharges at x = 5.15 m. | 30 |
| Figure 4.2(a) | Vertical velocity profiles for no bed material at a constant discharge of $6.4823 \times 10^{-3}$ $m^3/s$ and varying slopes at x = 3.15 m. | 31 |
| Figure 4.2(b) | Vertical velocity profiles for no bed material at a constant discharge of $6.4823 \times 10^{-3}$ $m^3/s$ and varying slopes at x = 4.15 m. | 31 |
| Figure 4.2(c) | Vertical velocity profiles for no bed material at a constant discharge of $6.4823 \times 10^{-3}$ $m^3/s$ and varying slopes at x = 5.15 m. | 32 |
| Figure 4.3(a) | Vertical velocity profiles for sunboard at a constant slope of 0.004 and varying discharges at x = 3.15 m. | 32 |

| | | |
|---|---|---|
| Figure 4.3(b) | Vertical velocity profiles for sunboard at a constant slope of 0.004 and varying discharges at x = 4.15 m. | 33 |
| Figure 4.3(c) | Vertical velocity profiles for sunboard at a constant slope of 0.004 and varying discharges at x = 5.15 m. | 33 |
| Figure 4.4(a) | Vertical velocity profiles for sunboard at a constant slope of 6.4823 $\times 10^{-3}$ $m^3/s$ and varying slopes at x = 3.15 m. | 34 |
| Figure 4.4(b) | Vertical velocity profiles for sunboard at a constant slope of 6.4823 $\times 10^{-3}$ $m^3/s$ and varying slopes at x = 4.15 m. | 34 |
| Figure 4.4(c) | Vertical velocity profiles for sunboard at a constant slope of 6.4823 $\times 10^{-3}$ $m^3/s$ and varying slopes at x = 5.15 m. | 34 |
| Figure 4.5(a) | Vertical velocity profiles for Plastic fibre mat at a constant slope of 0.004 and varying discharges at x = 3.15 m. | 35 |
| Figure 4.5(b) | Vertical velocity profiles for Plastic fibre mat at a constant slope of 0.004 and varying discharges at x = 4.15 m. | 35 |
| Figure 4.5(c) | Vertical velocity profiles for Plastic fibre mat at a constant slope of 0.004 and varying discharges at x = 5.15 m. | 35 |
| Figure 4.6(a) | Vertical velocity profiles for Plastic fibre mat at a constant slope of 6.4823 $\times 10^{-3}$ $m^3/s$ and varying slopes at x = 3.15 m. | 36 |
| Figure 4.6(b) | Vertical velocity profiles for Plastic fibre mat at a constant slope of 6.4823 $\times 10^{-3}$ $m^3/s$ and varying slopes at x = 4.15 m. | 36 |
| Figure 4.6(c) | Vertical velocity profiles for Plastic fibre mat at a constant slope of 6.4823 $\times 10^{-3}$ $m^3/s$ and varying slopes at x = 5.15 m. | 37 |
| Figure 4.7(a) | Variation of Manning's *n* with velocity at a constant slope of 0.004 and varying discharges for no bed material. | 39 |
| Figure 4.7(b) | Variation of Manning's *n* with velocity at a constant slope of 0.004 and varying discharges for no sunboard. | 39 |
| Figure 4.7(c) | Variation of Manning's *n* with velocity at a constant slope of 0.004 and varying discharges for plastic fibre mat. | 39 |
| Figure 4.8(a) | Variation of Manning's *n* with velocity at a constant discharge of 6.4823 $\times 10^{-3}$ $m^3/s$ and varying slopes for no bed material. | 40 |
| Figure 4.8(b) | Variation of Manning's *n* with velocity at a constant discharge of 6.4823 $\times 10^{-3}$ $m^3/s$ and varying slopes for sunboard. | 40 |

| | | |
|---|---|---|
| Figure 4.8(c) | Variation of Manning's *n* with velocity at a constant discharge of $6.4823 \times 10^{-3}\ m^3/s$ and varying slopes for plastic fibre mat. | 40 |
| Figure 4.9(a) | Variation of Chezy's *C* with velocity at a constant slope of 0.004 and varying discharges for no bed material. | 41 |
| Figure 4.9(b) | Variation of Chezy's *C* with velocity at a constant slope of 0.004 and varying discharges for no sunboard. | 41 |
| Figure 4.9(c) | Variation of Chezy's *C* with velocity at a constant slope of 0.004 and varying discharges for plastic fibre mat. | 41 |
| Figure 4.10(a) | Variation of Chezy's *C* with velocity at a constant discharge of $6.4823 \times 10^{-3}\ m^3/s$ and varying slopes for no bed material. | 42 |
| Figure 4.10(b) | Variation of Chezy's *C* with velocity at a constant discharge of $6.4823 \times 10^{-3}\ m^3/s$ and varying slopes for sunboard. | 42 |
| Figure 4.10(c) | Variation of Chezy's *C* with velocity at a constant discharge of $6.4823 \times 10^{-3}\ m^3/s$ and varying slopes for plastic fibre mat. | 42 |
| Figure 4.11(a) | Variation of Manning's *n* with aspect ratio at a constant slope of 0.004 and varying discharges for no bed material. | 43 |
| Figure 4.11(b) | Variation of Manning's *n* with aspect ratio at a constant slope of 0.004 and varying discharges for sunboard. | 43 |
| Figure 4.11(c) | Variation of Manning's *n* with aspect ratio at a constant slope of 0.004 and varying discharges for plastic fibre mat. | 43 |
| Figure 4.12(a) | Variation of Manning's *n* with aspect ratio at a constant discharge of $6.4823 \times 10^{-3}\ m^3/s$ and varying slopes for no bed material. | 43 |
| Figure 4.12(b) | Variation of Manning's *n* with aspect ratio at a constant discharge of $6.4823 \times 10^{-3}\ m^3/s$ and varying slopes for sunboard. | 43 |
| Figure 4.12(c) | Variation of Manning's *n* with aspect ratio at a constant discharge of $6.4823 \times 10^{-3}\ m^3/s$ and varying slopes for plastic fibre mat. | 43 |
| Figure 4.13(a) | Variation of Chezy's *C* with aspect ratio at a constant slope of 0.004 and varying discharges for no bed material. | 44 |
| Figure 4.13(b) | Variation of Chezy's *C* with aspect ratio at a constant slope of 0.004 and varying discharges for sunboard. | 44 |
| Figure 4.13(c) | Variation of Chezy's *C* with aspect ratio at a constant slope of 0.004 and varying discharges for plastic fibre mat. | 44 |

Figure 4.14(a) Variation of Chezy's *C* with aspect ratio at a constant discharge of $6.4823 \times 10^{-3}$ $m^3/s$ and varying slopes for no bed material. 44
Figure 4.14(b) Variation of Chezy's *C* with aspect ratio at a constant discharge of $6.4823 \times 10^{-3}$ $m^3/s$ and varying slopes for sunboard. 44
Figure 4.14(c) Variation of Chezy's *C* with aspect ratio at a constant discharge of $6.4823 \times 10^{-3}$ $m^3/s$ and varying slopes for plastic fibre mat. 44
Figure 4.15(a) Variation of Manning's *n* with Chezy's *C* at a constant slope of 0.004 and varying discharges for no bed material. 45
Figure 4.15(b) Variation of Manning's *n* with Chezy's *C* at a constant slope of 0.004 and varying discharges for sunboard. 45
Figure 4.15(c) Variation of Manning's *n* with Chezy's *C* at a constant slope of 0.004 and varying discharges for plastic fibre mat. 45
Figure 4.16(a) Variation of Manning's *n* with Chezy's *C* at a constant discharge of $6.4823 \times 10^{-3}$ $m^3/s$ and varying slopes for no bed material. 46
Figure 4.16(b) Variation of Manning's *n* with Chezy's *C* at a constant discharge of $6.4823 \times 10^{-3}$ $m^3/s$ and varying slopes for sunboard. 46
Figure 4.16(c) Variation of Manning's *n* with Chezy's *C* at a constant discharge of $6.4823 \times 10^{-3}$ $m^3/s$ and varying slopes for plastic fibre mat. 46
Figure 4.17(a) Comparison between *n* and velocity for all three materials at constant slope. 47
Figure 4.17(b) Comparison between *n* and velocity for all three materials at constant discharge. 47
Figure 4.18(a) Comparison between *C* and velocity for all three materials at constant slope. 48
Figure 4.18(b) Comparison between *C* and velocity for all three materials at constant discharge. 48

## GLOSSARY

| | |
|---|---|
| h | Flow depth |
| A | Area of cross-section |
| P | Wetted perimeter |
| v | Mean flow velocity |
| R | Hydraulic radius |
| S | Slope |
| b | Width of the channel |
| T | Top Width |
| $f$ | Darcy Weisbach's friction factor |
| $n$ | Manning's roughness co-efficient |
| $C$ | Chezy's roughness co-efficient |
| Q | Discharge |
| $C_V$ | Velocity co-efficient |
| $C_D$ | Co-efficient of discharge for venturimeter |
| g | Acceleration due to gravity |
| $\Delta h$ | Differential manometric head |
| $S_m$ | Specific gravity of mercury |
| S | Specific gravity of the flowing fluid |
| $x$ | Manometric head observed in venturimeter |
| $F_r$ | Froude's number |
| $m$ | Adjustment factor for meanders |
| $y_c$ | Critical depth |
| $R_e$ | Reynold's number |
| $\rho$ | Density of fluid |
| $\mu$ | Dynamic viscosity of fluid |

# CHAPTER 1

# INTRODUCTION

## 1.1 Definition

Various conveyance structures of different cross-sections are used for the transportation of liquids from one location to another. The flow through the structures which are open at the top and the surface of liquid is in direct contact with the atmospheric pressure is known as open-channel flow and such structures or conduits are known as open-channels. Various examples of open channel flow are river water flow, run-off, stream flow etc. Some applications of the open channel flow are used for practical importance. Examples are, determining depth of flow in a river etc., determination of changes in flow depth due to weirs, spillways etc., determination of run-off and changes in flow parameters due to channel transitions. Open channels can be of various types depending on their channel characteristics and cross-section and thus the problems of open-channel flow are relatively harder to analyze as it is not easy to determine the cross-section area in majority of open channels like rivers.
Main characteristics of open-channel flow are:

- Pressure is mostly hydrostatic and constant along the water surface.
- Gravity drives the flow in an open-channel.

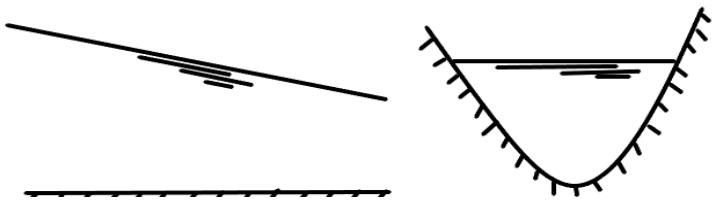

Figure 1.1 Typical representation of an open channel-flow

Factors influencing flow in open channels are:

- Type of channel
- Flow depth
- Flow velocity
- Channel slope
- Channel bed roughness

## 1.2 Classification of open channels

### 1.2.1 Man-made and natural channels

Natural channels are formed by natural alluvial processes whereas man-made channels are constructed to attain the desired flow.

Natural streams, rivers etc. are the examples of natural channels whereas lined canals are an example of man-made channels.

### 1.2.2 Prismatic and non-prismatic channels

The channels in which the cross-sectional parameters such as shape, slope etc. remain constant along the length of channel are known as ‘prismatic channels’ whereas the channels in which cross-sectional features vary along length are known as non-prismatic channels. It is important to note that most of the man-made channels are prismatic whereas all natural channels are non-prismatic.

### 1.2.3 Rigid and mobile boundary channels

The channels with non-deformable boundaries are known as rigid boundary channels. The flow in such channels is such that shape of channel does not depend on the flow parameters and no major deformation processes like scouring, erosion etc. occur at the channel boundary. The geometry of such channels remains constant with time. Lined channels are an example of rigid boundary channel.

The channels in which the boundaries are subject to significant erosion or scouring processes and the flow carries alluvial matter in suspension are known as mobile boundary channels. The geometric properties of such channels such as bottom slope, shape etc. are dependent on interaction of flow with channel boundary and the geometry of such channels may vary with space and time.

### 1.2.4 Based on the shape of channel, they may be classified as –

- Trapezoidal channel
- Rectangular channel
- Circular channel
- Triangular channel
- Parabolic channel

## 1.3 Types of open-channel flow

Figure 1.2 Open Channel flow (Source : https://www.mouthshut.com/product-reviews/Bhakra-Dam-Bilaspur-Photos-925753252)

### 1.3.1 Steady and unsteady flow

The flow in which hydraulic parameters like discharge, depth etc. do not change with time is termed as steady flow while flow in which the flow parameters vary with time is termed as unsteady flow. E.g.- flood flow.

### 1.3.2 Uniform and non-uniform flow

The flow in which the flow parameters such as discharge or depth do not change along the flow length is termed as uniform flow whereas the flow in which the flow parameters vary along the flow length is termed as non-uniform flow. E.g.,- flow in a prismatic channel at a constant discharge.

### 1.3.3 Critical, subcritical and supercritical flow

Froude number is a dimensionless parameter used to classify open channel flow into critical, supercritical and sub-critical flow. It depicts the ratio of gravitational forces to the inertial forces and is given by:

$$F_r = \frac{V}{\sqrt{gD}} \qquad (1.1)$$

where V- flow velocity, D- hydraulic depth and g- acceleration due to gravity

Critical depth, $y_c$, is depth corresponding to minimum specific energy for a particular discharge. The flow where the flow depth is equal to the critical depth is termed as critical flow and $F_r = 1$, in case of critical flow. Flow where flow depth is less than critical depth and slope is lesser than critical slope, is termed as supercritical flow. This type of flow occurs at relatively shallower depths and is categorised as rapid flow for which Froude number, $F_r > 1$.

The flow where flow depth is greater than critical depth is termed as subcritical flow and is categorised as slow flow and for which Froude number, $F_r < 1$.

### 1.3.4 Laminar, turbulent and transitional flow

Laminar flow is the flow in which the fluid moves in laminas or layers sliding over one another and no lateral mixing is observed. The velocity of fluid particles at any point in a laminar flow is constant at any point.

The flow in which the velocity of fluid particles is not constant and varies considerably in direction and magnitude is termed as Turbulent flow. It is characterised by eddies formation. Reynolds number, $R_e$ may be defined as the ratio of inertial and viscous forces and is a dimensional parameter used to classify laminar and turbulent flows.

$$R_e = \frac{\rho VR}{\mu} \qquad (1.2)$$

where ρ- fluid density, V- velocity of flow, R- hydraulic radius and μ is the dynamic viscosity of the fluid.

The flow is termed as laminar for $R_e < 500$, turbulent for $R_e > 12500$ and

Transitional for $500 < R_e < 12500$ (Chow 1959)

### 1.3.5 Gradually-varied, rapidly-varied and spatially-varied flow

These are the types of non-uniform flows. When the change in depth, caused by an obstruction is large over a relatively shorter reach, the flow is called rapidly-varied flow. When change in flow depth is gradual over a longer distance, it is termed as gradually varied flow. Spatially-varied flow can be steady or unsteady. This type of flow can be observed when water is added or taken out from a channel along the flow direction.

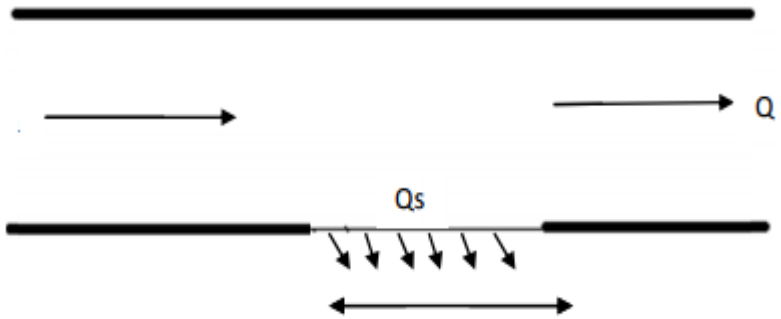


Figure 1.3 Diagrammatic representation of spatially-varied flow

## 1.4 Geometric elements of open-channel flow

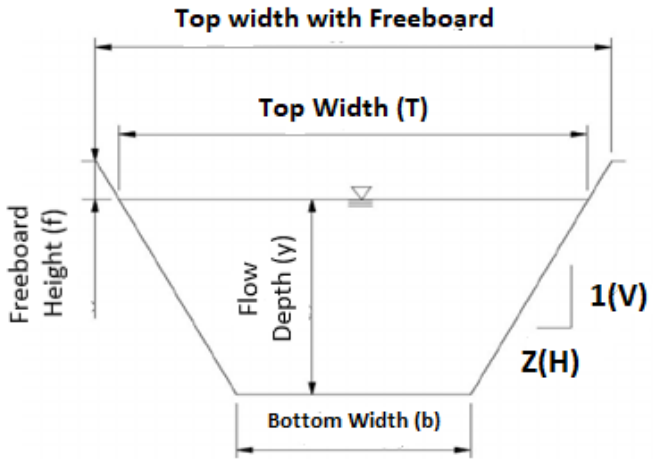


Figure 1.4 Geometric representation of open channel

- Depth of flow (y) - The vertical distance between the lowest point in channel to the free water surface, normal to the flow direction is called flow depth.
- Stage (H) - The vertical distance from datum to the free surface is called stage. If lowest point is taken as datum, stage is equal to the depth of flow.
- Top width (T) - The channel width at free surface is known as top width.
- Flow area (A) - The area of any section normal to the flow direction is known as flow area.
- Wetted perimeter (P) - The length of wetted surface normal to the flow direction is known as wetted perimeter.
- Hydraulic mean radius (R) - Ratio of flow area to wetted perimeter is termed as Hydraulic Mean Radius.

$$R = A/P \tag{1.3}$$

- Hydraulic depth (D) - Ratio of flow area to top width is termed as hydraulic mean depth.

$$D = A/T \tag{1.4}$$

- Discharge (Q) - The volumetric flow rate through a given cross-section area is known as discharge.

$$Q = A.V \tag{1.5}$$

where A is the are of flow and V is the flow velocity

- Manning's coefficient (*n*) - It is a dimensionless parameter used to signify the amount of resistance or friction applied to the flow by the channel.
- The ratio between width of channel section (b) and depth of flow (h) is termed as aspect ratio.

## 1.5 Geometric properties of different types of channel

### 1.5.1 Rectangular channel

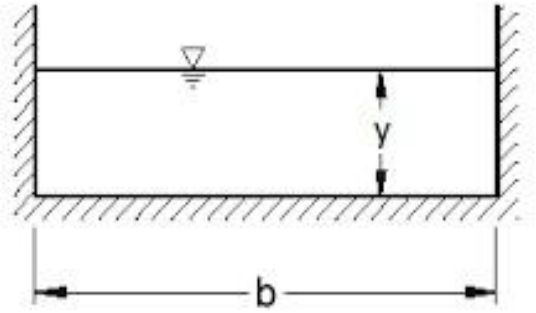


Figure 1.5 Cross-Section of a rectangular channel
(Source : www.brainkart.com)

Area of flow, A = b.y (1.6)

Top width, T = b

Wetted perimeter, P = (b+2y) (1.7)

Hydraulic mean radius, $R = \frac{by}{(b+2y)}$ (1.8)

Hydraulic depth, D = y (1.9)

### 1.5.2 Trapezoidal channel

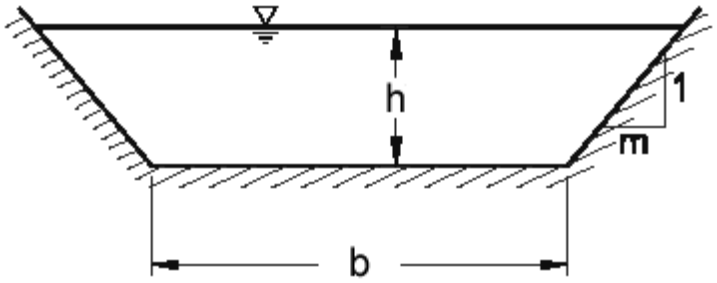


Figure 1.6 Cross-section of a trapezoidal channel
(Source : www.brainkart.com)

Area of flow = (b + mh).h (1.10)

Top width (T) = b + 2mh (1.11)

Wetted perimeter (P) = $b + 2h\sqrt{1 + m^2}$ (1.12)

Hydraulic radius (R) = $\frac{(b+mh)h}{b+2h\sqrt{1+m^2}}$ (1.13)

Hydraulic mean depth (D) = $\frac{(b+mh)h}{b+2mh}$ (1.14)

### 1.5.3 Circular channel

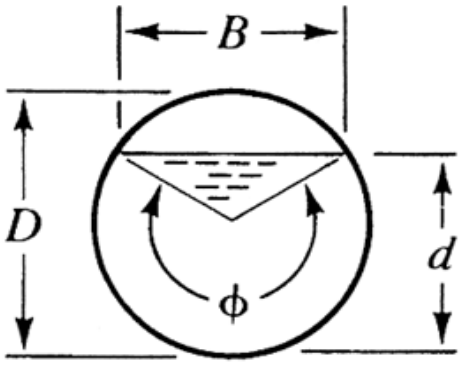


Figure 1.7 Circular channel cross-section
(Source : www.brainkart.com)

Area of flow, A = $(\emptyset - \mathrm{Sin}\emptyset)\frac{D^2}{8}$ (1.15)

Top width, T = $D.\mathrm{Sin}\frac{\emptyset}{2}$ (1.16)

Wetted perimeter, P = $\frac{\emptyset D}{2}$ (1.17)

Hydraulic radius, R = $\left(1 - \frac{\mathrm{Sin}\,\emptyset}{\emptyset}\right)\frac{D}{4}$ (1.18)

Hydraulic depth, D = $\left[\frac{\emptyset - \mathrm{Sin}\emptyset}{\mathrm{Sin}\frac{1}{2\emptyset}}\right]\frac{D}{8}$ (1.19)

### 1.5.4 Triangular Channel

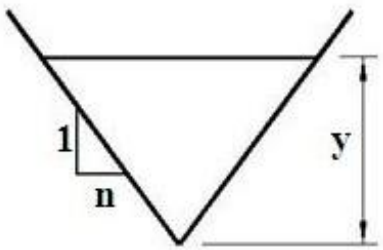


Figure 1.8 Triangular channel cross-section
(Source : www.brainkart.com)

Area of flow, $A = ny^2$ (1.20)

Top width, $T = 2ny$ (1.21)

Wetted perimeter, $P = 2y\sqrt{1 + n^2}$ (1.22)

Hydraulic radius, $R = \frac{ny}{2\sqrt{1+n^2}}$ (1.23)

Hydraulic depth, $D = 0.5y$ (1.24)

## 1.6 Manning's equation for open-channel flow

Manning's equation has been used by engineers to analyze and study open channel flows and is a semi-empirical relation used for simulation of water flows in various types of open channel flows. This equation was first put forth by Robert Manning in the year 1889 and is used mainly for steady uniform flow regimes.

$$Q = \frac{1}{n} A R^{2/3} S^{1/2} \quad (1.25)$$

where Q is the discharge , A is the cross-sectional flow area, R is the hydraulic mean radius, Sis the slope and *n* is Manning's coefficient.

## 1.7 Chezy's co-efficient of roughness (*C*)

Chezy's Coefficient is another important roughness parameter in open channel flow. The flow velocity by Chezy's equation is given by –

$$V = C\sqrt{RS} \quad (1.26)$$

Re-arranging equation 1.26, chezy's coefficient can be calculated by –

$$C = \frac{V}{\sqrt{RS}} \quad (1.27)$$

Where V is flow velocity in m/s, R is hydraulic mean Radius and S is the slope of channel bed.

### 1.8 Relevance of Manning's *n*

Manning's equation and roughness coefficients are widely used for simulating open-channel flows. Manning's roughness co-efficient amounts for the interaction of various flow parameters with the channel and hence are an utmost important tool in analysing various aspects of an open channel flow. Manning's roughness coefficient accounts for the various processes that constitute an open channel flow like scouring, flow depth, flow velocity, stress distribution and sediment transport through a single value. Flow velocity is one of the main characteristics influenced by the roughness of channel and hence the knowledge of roughness coefficients for various types of channels helps in the analysis and hence acquiring the required flow as per the required purpose. In other words, roughness coefficients account for the roughness parameters and hence, their effect on the open channel flow.

### 1.9 Objectives

The work is aimed at determination of Roughness coefficients for different bed materials. The major objectives are -

- To determine the Manning's and Chezy's roughness coefficients for different bed materials.
- To determine the velocity distribution over these bed materials and study the variations of velocity with other flow parameters.

### 1.10 Organization of Thesis

This research work has been divided into 5 chapters

- Chapter 1 is an introduction chapter describing open-channel flow and various associated parameters. This chapter gives a layout for thesis.
- Chapter 2 represents the review on various works done in the field of different bed roughness and their effect on the flow.

- Chapter 3 deals with the experimental setup, procedure and bed material characteristics used in the experimental work.
- Chapter 4 includes results and discussions part from the experimental procedures performed.
- Chapter 5 shows the significant conclusions drawn from different parts of chapter in this thesis.

# CHAPTER 2

# LITERATURE REVIEW

The current presents a review of different works done and the importance of roughness parameters that effect flow parameters in an open channel flow. Different observations pertaining to different flow parameters and conditions have been presented for a more detailed understanding of open channel flow.

## 2.1 Open Channel Flow and Hydraulic Resistance

For stimulation and regulation of flow in a stream or river section, hydraulic engineers often utilize their knowledge about conveyance and the flow resistance parameters that affect the flow directly or indirectly. Many well defined equations and relations have been developed and used for the same purpose. A lot of research work and studies have been undertaken to understand the overall effect and impact of various roughness in a channel i.e., bed and side roughness. Channel roughness hinders the flow by impacting various geometrical and hydraulic parameters constituting it. Flow resistance in open channels is a complex parameter as we lack accurate methods to determine it.

Roughness in a channel is impacted by many factors such as suspended sediment load, type of sediments, type of bed form or roughness, channel sinuosity as well as variations in depth and width of the channel in consideration.

Cowan (1956) extensively performed an array of studies involving retardance factors. He, thus established a procedure to estimate the value of Manning's *n* by setting a baseline value of *n* for natural bed material in a straight and uniform channel. Various modifications for channel related geometrical and retardance parameters like channel bed irregularities, variations in channel geometry, type and density of vegetation are applied and the sum of these factors is added to the base value and multiplied by channel meandering adjustment factor *m* to obtain a cumulative value for Manning's roughness co-efficient. The *n* values as per the method for modified streams have been given in various work manuals. The following equation represents the postulation provided by Cowan:

$$n = (n_0 + n_1 + n_2 + .. + n_n)m \qquad (2.1)$$

where $n_o$ – base value of *n* for a straight, uniform channel , *m* – adjustment for meanders and $n_1, n_2, \ldots, n_n$ – adjustments for roughness factors other than meanders.

First the base value of *n* is determined and the modifications for variations in channel geometry and vegetation type are applied. Equation (2.1) can then be used to approximate the Manning's *n* for a certain channel.

Fenzl and Davis (1964) found the roughness or retardance coefficient '*n'* to increment with depth of flow, when they subjected the vegetation in a flow with depth considerably less than the tallness of vegetation for low conveyance rate. For this situation, there was next to zero redirection in plant stems. But for submerged condition the upright position of vegetation was disturbed and *n* values noticed a variation with the product of average flow velocity(V) and hydraulic radius(R) of the channel. *n* showed an inversely proportional relationship with VR until a point after which roughness criteria and configuration stayed unchanged. *n* tended to stay constant with further increment in VR values.

Kouwen et al. (1969) planted styrene strips simulating vegetation in a laboratory flume and plotted velocity profiles for different flow conditions. They inferred that the velocity remained constant inside the vegetation layer whereas the velocity profile was observed to follow logarithmic law above it.

Li and Shen (1973) led an extraordinary investigation on the stream of water in vegetated open channels with different examples of collection of vegetation and found that tall vegetation assembled into staggered arrangements are considerably more viable in elevating the roughness coefficient and consequently on reducing conveyance rate than some other example for a similar vegetation thickness. They additionally saw that tall vegetation rows planted at right angles to flow direction greatly hindered the flow.

Petryk and Bosmajian (1975) utilized the model of a straightforward flow retardance approach for developing emergent vegetation conditions to foresee Manning's *n*. They saw that Manning's *n* was directly proportional to two-third power of the hydraulic radius (R), for vegetated channel with uniform vegetation thickness. They asserted that for the flow course through vegetation, drag was the fundamental force that offered retardance to the flow instead of cumulative shear force on the channel boundaries.

Thompson and Roberson (1976) used small diameter cylinders, simulating vegetation roughness ,to develop an analytical model for the purpose of determining resistance co-

efficient which in turn can be utilized to solve various equations such as Manning's, Chezy's or Darcy-Weisbach equation for open channel flows.

Kao and Barfield (1978) utilized plastic strips in molten paraffin to simulate the characteristic vegetation. They reasoned that, in a thickly vegetated channel, drag constraint by vegetation blades is a prevailing feature for selection of Manning's *n* under the conditions of shallow emergent flow. They observed that the flow depth and velocity of flow followed a directly proportional realationship with the drag resistance and hence the roughness coefficient until the conditions of submerged flow were achieved. After that, roughness was observed to follow an inversely proportional relationship with the flow depth and velocity.

Kouwen and Li (1980) put forth a general procedure to estimate Manning's *n*, keeping the various physical flow parameters and properties of the vegetation under consideration. They observed that comparative roughness and the type of vegetation greatly influenced the roughness parameters in the flow regime and hence *n* was a function of these two criteria. They also developed a procedure to estimate the flexural stiffness of different kinds of vegetation.

Temple (1982) stated an improvement over the existing methods for deterimination of resistance offered to a flow regime by vegetation in an open channel. He attempted to relate the flow resisting potential of a certain vegetation directly to various available physical parameters of flow under consideration. His method has been used extensively in the design of vegetated streams or channels for tractive force.

Temple (1986) extensively studied the flow in vegetated open channels and various factors affecting it. He came up with a two-layer velocity profile for such channels and observed some trends suggesting the role of vegetation in hindering the flow. He observed that for depths less than the deflecting height, velocity distribution stays fairly constant and is affected only by vegetation thickness or bed slope but depends on momentum transfer during turbulent shear under submerged conditions.

Sumer et al. (1996) performed studies in a tilting flume and developed velocity profiles for a moving bed with four distinct types of sediments of different sizes. They observed the velocity profiles in relation to sheet layer and observed that under the sheet layer, velocity

profiles seemed to satisfy power law but followed a logarithmic trend outside the sheet layer near the bed.

Ikeda and Kanawaza (1996) used flexible vegetation and collected the logitudnal velocity data using an ADV. They observed a point of inflection in the velocity profile, close to the surface of vegetation layer. They also inferred that the maximum value of logitudnal components of turbulence and shear stress is found near the top of vegetation layer whereas it decreased above the vegetation towards the free surface.

Anwar (1996) attempted to evaluate the effects of uncertainities in flow on velocity distribution. He performed a number of experiments in shallow coast water and recorded the mean velocity profiles of the tidal flows during the acceleration and deceleration phases. He was able to state three different regions in the profiles, (i) Inner region (near bed), (ii) outer region and (iii) Overlapping region. He also stated that the trends in the overlapping region satisfied the logarithmic law while the trends in outer region obeyed defect law.

Pang (1998) performed experiments on straight reaches in a compound channel under isolated and interacting conditions. He found out that the discharge distribution between the floodplain and main channel was in accordance with the energy loss, which could be stated in the form of resistance coefficient. He also stated that Manning's roughness coefficient *n* was not only a denotion of characteristics of roughness, but also impacted energy loss occurring in the flow. He observed that the value of *n* with the same bed form in floodplain and main channel had varying values when the flow depth varied in the section.

Cheng et al. (1998) stated that channel having sediments in abundance or vegetation creates large scale roughness. The flow through the stem layer is almost uniform whereas in the surface layer it is logarithmic over such a rough bed may differ considerably from those over smooth boundaries. A no slip condition occurs if the channel bed is smooth and impermeable. On the other hand, presence of vegetation obstructs the lower portion of channel flow functioning as a porous medium to reduce the flow velocity. This produces a two layered velocity profile: one above vegetation called surface layer and the second within the vegetation called stem or vegetation layer. The two layers interact in a manner that is very similar to the plane mixing layer rather than the boundary layer. The flow through the stem layer is almost uniform whereas in the surface layer it is logarithmic.

Wu et al. (1999) used a horsecoir mattress to in their experimental procedure to simulate vegetation on a channel and studied variation of roughness with the flow depth. From the test results, they inferred that for emergent flow, roughness coefficient decrease with increment with flow depth while the coefficient seems to increase at small depths but decreases to a constant value as water level keeps on increasing. They proposed a model based on force equilibrium to estimate the drag due to vegetation and using the model, then used Manning's equation to convert drag coefficient into roughness co-efficient. The data was compared with previous studies and tests and the results pointed out a consistent variation trend between $R_e$ and drag coefficient.

Righetii and Armanini (2002) stated that values of roughness coefficients in a thinly scattered vegetation in open channel flows depend on submergence. They inferred that the values were higher during the wet seasons of the year as higher flows would cause the vegetation to give way and submerge whereas the values of co-efficients are much higher during the dry seasons with minimal flows due to only partial submergence of vegetation.

Yang et al. (2005) utilized the Flood Channel Facility data for many main channels and floodplains of varying geometries and roughness characteristics to put forth some relationships between local, overall and zonal roughness coefficients (*n* and *f).* They observed that the relationship between Reynold's number ($R_e$) and '*f'* is different in single and compound channels. They also pointed that for smooth compound channels, local roughness coefficients remain fairly constant upto a certain relative depth and vary in the main channel and floodplains while the coefficients decreased with an increase in relative depth in case of rough compound channels.

Wilkerson (2007) used wooden dowels to represent rigid vegetation in his studies. The dowel patterns used were taken to mirror the effects of willow post systems i.e., array of rigid cylinders placed along bank to reduce bank erosion. In addition, he presented an analytical model for prediction of depth-averaged velocity distribution in channels of varying geometric cross-section. The analytical model was developed on the basis of wake phenomenon and applies to channel flows with fully submerged and unsubmerged rigid cylinders simulating vegetation. He used the analytical model to predict the depth-averaged velocity data($U_{pred}$), and then verified it with the velocity data observed in various physical models ($U_{observed}$). The discrepancy ratios, $U_{pred}$ /$U_{obsd}$, were typically between 0.80 and 1.20. Results concluded

that significant variables for reduction of local velocities are vegetation height, diameter,density and the pattern or configuration of the vegetation under consideration.

Yang et al. (2007) studied the flow resistance characteristics of overbank and inbank flows by observing different resistance coefficients (*f, n and C*). For the purpose, they performed a series of experiments on the rough bed of a compound channel and floodplains. They noted that for overbank flows over a rough bed, the variation of roughness parameters with the water depth is very complex and also proposed some methods for the estimation of composite roughness from the experimental and field data for thr compound channels.

Rhee et al. (2007) utilized three characteristic vegetations Zoysia matrella, Pennisetum alopecuroides (L.) spreng and Phragmites communis trin, in flume tests. After performing the experiments, they inferred that green plants exhibit a higher roughness potential compared to the lethargic vegetation. Additionally, they tried to estimate Manning's *n* for green plants that is 0.012 and when compared with the lethargic vegetation (0.001), was much higher.

Huai et al. (2009) studied and evaluated the vertical velocity distribution in an open channel flow with submerged vegetation. A 3D Micro ADV was used to measure the vertical velocity and turbulence trends of steady uniform flow. The vertical velocity and shear stress distribution were then obtained for sets of different vegetation arrangements in the channel. They observed that the vertical velocity profiles consisted of three regimes within the vegetation (i.e. upper non-vegetated layer, the outer layer and the bottom layer within).

Greco et al. (2013) proposed the below equation that suggests the relation between entropy parameter for low depth and the roughness co-effecient.

$$\left(\frac{y_o}{y_m}\right)_{calibrated} = 0.094 i\% e^{[0.445 l_n\ (i\%) - 0.278]} \left(\frac{D}{d}\right) \qquad (2.2)$$

In this equation, $\left(\frac{y_o}{y_m}\right)_{calibrated}$ is the ratio between the positions where velocity is zero and maximum.

Dash et al. (2013) examined energy loss in flows due to varying flow conditions. As per the examinations made, some critical deductions were made. Most huge among them was reliance of Manning's *n* on flow depth at various sections. It is seen that Manning's *n* is

specifically correspondant to the flow depth. He exhibited the plots and diagrams in his evaluations which unmistakably show that roughness coefficient increases with an increment in the depth of flow, which is for the most part due to more energy losses in a wider channel carrying shallow depths than narrow channels carrying higher depths and meandering channels expend more energy with increment in flow depth. In this way, Manning's coefficient '*n*' isn't just a determinant of roughness of a channel yet in addition decides the energy transfer in the flow.

Das et al. (2016) performed experiments in a 6m long and 0.3m wide rectangular glass flume with metal bed at Water Resource laboratory in Assam down town University, Guwahati. Different bed conditions were made artificially, using grass carpet and coconut coir mat for rough bed condition and PVC material and original metallic bed for smooth bed condition. The flow depths were measured and various flow parameters were calculated. Flow conditions were varied with slope and discharge being constant under different conditions. The mathematical modelling of bed roughness with respect to variation of flow parameters for different bed conditions were presented. The spreadsheet calculations were performed in order to obtain the values of Manning's roughness coefficient and other flow parameters. Relation of Manning's roughness coefficient with depth of flow, and Froude's number are obtained using regression equations and graphical analysis. It was observed that the flow parameters vary with the variations of bed roughness in open channel flow. Manning's roughness coefficient also varies with the variation of open channel bed conditions.

**Flow depth and channel gradient:**

In view of the examinations done as such far, there is a solid reliance of base value n and flow height. In the territories where there is no vegetation and consequently no check, the roughness coeffecient diminishes with the increment in the height of flow. This reality is additionally proposed by these two conditions. In addition, because of the increased flow depth, the energy dissipates because the roughness turn out to be considerably minimal. Likewise channel roughness has an immediate connection with the channel slope. This just implies the sloping channels will bring down roughness and the other way around. Since slope is a decent determinant for the roughness, along these lines slope must be considered while choosing the base n.

**Degree of channel irregularity:** Roughness caused by disintegrated and scoured banks, anticipating focuses, be that as it may, can be represented by adding changes in accordance with the base estimation of *n*. Chow (1959) and Benson and Dalrymple (1967) demonstrate that seriously dissolved and scoured banks can expand values by as much as 0.02

**Variation in channel cross-section:** Steady changes found in the grain size estimation and different sizes do not influence the entropy changes. But vast and little cross segments exchange at times, or the fundamental flow infrequently moves from side to side, energy changes in accordance with the base n value

**Effect of obstructions**: Separated stones, flotsam and jetsam stores, logs, control shafts and towers, and extension wharfs that irritate the flow design in the channel increment *n* values. The measure of increment relies upon the state of the hindrance, its size in connection to different roughness components in the cross area, the number, course of action, and separating of the obstacles, and the extent of flow speed (Aldridge and Garrett, 1973)

## 2.2 Critical Review

Manning's roughness is an important characteristic that defines the flow development in an open channel. Channel geometry, bed roughness, discharge, slope and sediment concentration are some parameters that greatly affect the roughness characteristics of a channel. Hence, Manning's coefficient provides a farther insight on development of flow in a compound open channel. It can be observed that manning's coefficient defines the velocity distribution and depth of flow under different bed roughness and is inversely proportional to the flow discharge while being directly proportional to the bed slope of the channel. The investigations carried out have tried to establish and re-investigate these trends.

# CHAPTER 3

# EXPERIMENTAL PROCEDURE AND SETUP

## 3.1 General

Experiments were conducted under controlled laboratory conditions in the Fluid Mechanics Laboratory of the Civil Engineering Department at Thapar University, Patiala, India in order to find out the impact of roughness characteristics of different bed materials on various hydraulic characteristics of open channel flow. The hydraulic characteristics of flow studied were hydraulic Manning's roughness coefficient, *n* and velocity distribution of flow over three types of bed materials. This chapter describes the experimental channel design, application of roughness elements and measurement techniques of experimental data on velocity of flow details of the various instruments used to measure the experimental data are also discussed in this chapter.

## 3.2 Experimental Channel Design

### 3.2.1 Tilting Flume

For the present study a straight simple channel in the form of a tilting flume having length 6 m, width 0.3 m and depth of 0.45 m is used. The tilting flume is made of metal frame with glass walls at the test reach. At the beginning of the flume just after inlet and before head gate (called stilling chamber), a series of baffle walls are installed for energy dissipation purpose, i.e., to reduce turbulence and to make water still before passing over the channel. Head gate reduces the waves if formed in the water body before it passes over the channel and in this way head-gate plays a vital role in maintaining uniform flow. Tailgate was provided just before end point of the flume for bed slope measurement purpose. The flume was supported on a hinge at the centre and made tilting by providing hydraulic jack arrangement at starting point of the flume. The plan view of the experimental channel used in the present study is shown in Fig. 3.1. The overall view of the flume with experimental set up is shown in Figs. 3.1 and 3.2.

Figure 3.1 Tilting flume at Water Resources Lab, Thapar University, Patiala

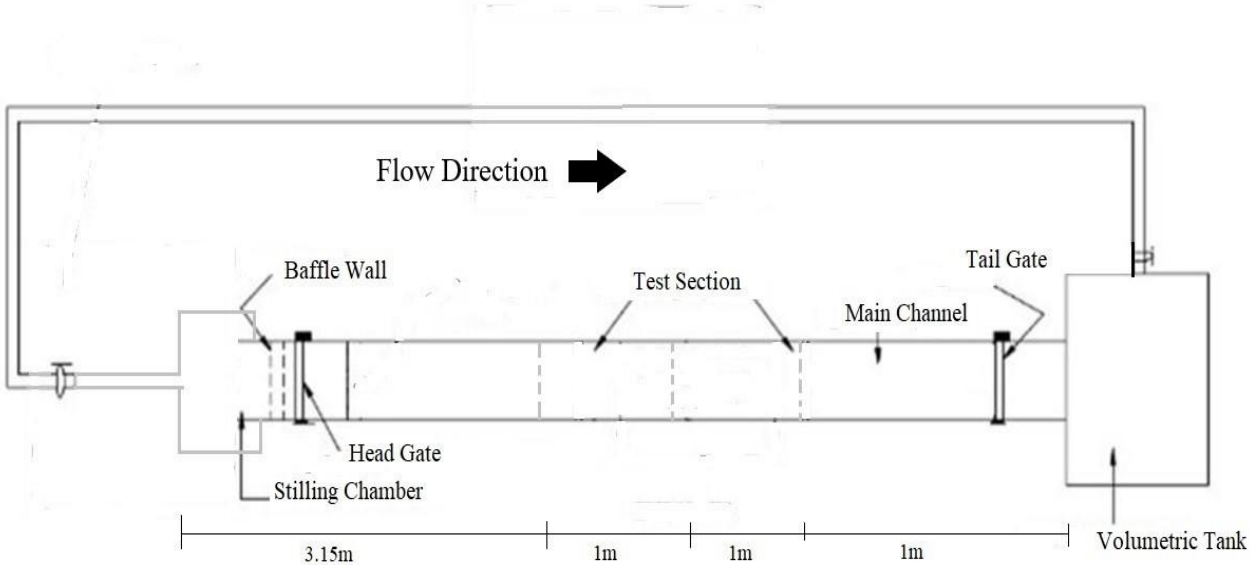


Figure 3.2 Schematic view of experimental setup

Table 3.1 Geometrical features of flume

| S. no. | Description | Parameters |
|---|---|---|
| 1. | Channel type | Straight |
| 2. | Geometry of Channel Section | Rectangular |
| 3. | Channel Base and Top width | 0.30m |
| 4. | Height of Channel | 0.45m |
| 5. | Length of test section | 3m |
| 6. | Length of whole Channel | 6m |
| 7. | Bed slope | 1 in 2.5 |

### 3.2.3 Water Conveyance System

The water supply system consists of a water tank, a re-circulating pipeline and a centrifugal pump coupled to a motor. The water is supplied to the flume from the rectangular water tank fitted with the recirculating pipeline using a centrifugal pump coupled to a motor to lift the water to the flume channel section. A delivery valve and a venturimeter are fitted to the pipeline for regulation of discharge through the flume channel. A vertical differential U-tube mercury manometer is connected to the throat and inlet of the venturimeter to measure the discharge. The water is recirculated in the flume to avoid any wastage.

Figure 3.3 Water supply motor

### 3.2.4 Pitot tube for velocity measurement

Figure 3.4 Pitot Tube

A micro pitot pitot tube with a diameter of 8mm along with a manometer were used for velocity calculation purposes. Pitot tube was fixed to a scale with vernier attachment and had a least count of 0.1mm. The pitot tube is faced towards the direction of flow to give the total pressure and surface holes give the static pressure. The pressures can be noted as the amount of water rising in the limbs of manometer. The difference between the water level in the two tubes is used to calculate the velocity using the relation-

$$V = C_v\sqrt{2g\Delta h} \quad (3.1)$$

where V- flow velocity, $C_v$- Coefficient of velocity, g- acceleration due to gravity and Δh is the difference between water levels in the two limbs of manometer. $C_v$ value of 0.80 was used for calculating velocity.

### 3.2.5 Venturimeter for discharge measurement

A venturimeter of size (50mm x 30mm) was fitted in the water supply pipe with its inlet and throat connected to a U-tube differential manometer containing mercury. The difference between the rise of manometric mercury is used to estimate and regulate the discharge in the flume, given by the relation –

$$Q = C_d \frac{A_1 A_2}{\sqrt{A_1^2 - A_2^2}} \sqrt{2g\Delta h} \quad (3.2)$$

where Q- actual discharge in $m^3$/sec, $C_d$- discharge coefficient of Venturimeter, g- acceleration due to gravity, $A_1$ - area of venturimeter at inlet in $m^2$, $A_2$ - area of venturimeter at throat section in $m^2$ and Δh is the differential manometric head in metre. $C_d$ value of 0.95 as given by the lab manual was considered for discharge calculation.

### 3.3 Experimental procedure

The main characteristic parameters to be measured in the experimental procedure were the velocity, discharge and bed slope of the flume channel. Discharge was calculated and regulated with the use of venturimeter. Three different discharge values corresponding to the $\Delta h$ values of 8.5, 9.5 and 10.5 cm, i.e., $6.1314 \times 10^{-3}$ $m^3/s$, $6.4823 \times 10^{-3}$ $m^3/s$, $6.8149 \times 10^{-3}$ $m^3/s$ respectively, were taken and fixed accordingly. Similarly, three different slope values of 1 in 1.5, 1 in 2.5 and 1 in 3.5 i.e., 0.00286, 0.04 and 0.0067 respectively were considered and adjusted with the help of hydraulic jack arrangement at the base of the flume. Two different materials were used for fabricating the flume channel bed and a test reach section of length 3m was fixed 1 away from the tail gate in flume. Velocity readings were taken at 3 sections, at every 1metre length along the channel test reach. Five runs of experiments were conducted for each material, designated E1 to E5, described in the table below-

Table 3.2 Experimental runs and their characteristic flow parameters

| Experiment | Characteristic parameters |
|---|---|
| E1 | $Q = 6.1314 \times 10^{-3}$ $m^3/s$, $S_1 = 0.004$ |
| E2 | $Q = 6.4823 \times 10^{-3}$ $m^3/s$ , $S_1 = 0.004$ |
| E3 | $Q = 6.8149 \times 10^{-3}$ $m^3/s$, $S_{1\,=}\, 0.004$ |
| E4 | $Q = 6.4823 \times 10^{-3}$ $m^3/s$, $S_2 = 0.00286$ |
| E5 | $Q = 6.4823 \times 10^{-3}$ $m^3/s$, $S_3$ = 1 in 0.0067 |

The first three runs designated E1 to E3 were conducted by varying discharges with a constant slope and last two runs designated E4 and E5 were conducted, fixing the discharge and varying the slopes. A total of 3 values of both discharge and slope were considered and the velocity profiles taken accordingly. Similarly, five runs of experiments were conducted for each of the materials. First set of five-run experiments was conducted without any fabrication of flume bed i.e., on a corroded steel bed, Second set of experiments was conducted after fabricating the flume bed with sunboard and third set of experiments was conducted after fabrication of flume bed with plastic polymer grass mats. Vertical velocity profiles were calculated for all the flow condition parameters with the help of a static pitot tube , for the calculation of manning's roughness coefficients for different types of bed materials. The experiments were performed under steady flow conditions and flow conditions were obtained by letting the water run through the channel for sometime and adjusting the head gate accordingly. The flow depths were measured after some intervals of time to make

the steady flow conditions were achieved. The depth of flow at a section was calculated using a pointer gauge with vernier attachment having a least count of 0.1mm. The bed was fabricated by fixing the different materials using various water tight adhesives.

### 3.4 Used Bed Materials

Table 3.2 Thickness of the used bed materials

| S.no. | Material | Thickness |
|---|---|---|
| 1. | Sunboard | 3mm |
| 2. | Plastic fiber mats | 12mm |

Sunboard is a strong, light and easily cut sheet material used for vinyl mounting, painting etc and has a smooth surface . It usually has an inner layer of polystyrene foam and a white claycoated paper on the outside.

Figure 3.5 Sunboard used as a bed form

The second fabrication material used was a plastic mat of 12mm thickness with a relatively rough and even surface , imitating vegetation. These types of mats are often used at the entrance of various buildings for dust trapping purposes. Being relatively flexible and rough as compared to the sunboard, plastic fibre mat was used to simulate very minial vegetation considering very small plastic fibre threads on its surface.

Both the materials were cut out to a size with a length of 3m and width equalling the flume channel width, i.e., 0.305 m or 30.5 cm. The materials were fixed to flume bed using superglue and various water-tight adhesives (m-seal). The water pressure would filtrate through the bed and the material strips had to be changed and fixed again after every two runs of experiments.

Figure 3.6 Plastic fibre mat used as a bed form

### 3.5 Slope Adjustment

For adjusting the channel bed slope, the hydraulic jack arrangement in the flume was used. The slope values were changed and recorded using two methods. The slope values were checked by measuring the difference between the water levels at both the ends in a single open pipe after placing it at both the flume ends. Then , the channel was flooded with water to check for the obtained slope value. The water depth at the two end points along the centre of test section was recorded using a point gauge with a least count of 0.1 mm which was mounted on a wooden frame and placed on two railing running on top of the flume along the flume length. The slope of the bed was found out by dividing the water depth difference at two ends of test section by the length of test section.

Figure 3.7 Hydraulic jack arrangement in the flume for changing slope

### 3.6 Obtaining Steady flow conditions in the flume

The laboratory flume used in the study is relatively short at 6.15m in length, and it is hence assumed the flow is allowed a free over-fall at the tail end. Steady flow conditions can be achieved by adjusting the tail gate and measuring flow parameters like flow depth and velocity at different time intervals to make sure that they do not change with time.

# CHAPTER 4

# RESULTS AND DISCUSSIONS

## 4.1 General

This chapter presents the various results of experimental investigations and their interpretation in order to understand the role of roughness parameters in regulating the different flow variables. The results will be discussed material-wise as discussed in chapter 3 and then interpreted collectively to establish and find out different inter-relationships and dependence of roughness parameters on flow variables. Five runs of experimental investigations were carried out for each of the bed material conditions and the roughness parameters calculated accordingly.

## 4.2 Variables and Flow parameters

In the present study, the various flow parameters observed and measured are depth of flow at 3 sections that were 1m apart ($h_1$, $h_2$, $h_3$), flow velocity in the direction of flow (V), area of flow (A), hydraulic radius (R), Manning's roughness coefficient (*n*) and Chezy's coefficient. The discharge was adjusted and measured using a venturimenter of cross-section 50mm x 30mm. The slope was adjusted and changed in different runs with the help of hydraulic jack arrangement provided in the flume apparatus and measured by appropriate method discussed in the previous chapter. The values of the parameters measured under the investigations are recorded in the following tables. The discharge was varied using the manomteric head of the differential U-tube manometer and three values of manometric head were considered for the purpose i.e., x = 8.5, 9.5 and 10.5. Since the manometric fluid (mercury) was heavier than water, equation 4.1 was used to calculated the differential head for the calculation of discharge. $S_m$

$$h = x\left(\frac{S_m}{S} - 1\right) \qquad (4.1)$$

where $S_m$ is the specific gravity of mercury = 13.66 , S is the specific gravity of flowing fluid i.e., water = 1.000, and *x* is the manometric head observed in venturimeter.

Thus, three discharge values were considered and varied in the different runs i.e., $Q_1$= 6.1314 × $10^{-3}$ $m^3$/s , $Q_2$= 6.4823 × $10^{-3}$ $m^3$/s and $Q_3$= 6.8149 × $10^{-3}$ $m^3$/s. Table 4.1 presents details of geometric and hydraulic parameters for flow without any bed material.

Table 4.1 Hydrological and Geometrical parameters for flow without any bed material

| Q ($\times 10^{-3}$ $m^3/s$) | S | h (mm) | b (m) | A ($m^2$) | P (m) | R=A/P | V (cm/s) | b/h |
|---|---|---|---|---|---|---|---|---|
| 6.1314 | 4 | 64.1 | 0.305 | 0.0196 | 0.4332 | 0.0452 | 31.8 | 4.76 |
| 6.4823 | 4 | 66.2 | 0.305 | 0.02018 | 0.4373 | 0.0461 | 32.9 | 4.61 |
| 6.8149 | 4 | 67.2 | 0.305 | 0.02051 | 0.4395 | 0.0467 | 34.0 | 4.54 |
| 6.4823 | 6.7 | 60.4 | 0.305 | 0.0184 | 0.4258 | 0.0438 | 35.7 | 5.05 |
| 6.4823 | 2.86 | 68.7 | 0.305 | 0.0209 | 0.4423 | 0.0474 | 31.1 | 4.43 |
| Q – Discharge, S – Slope in mm/m, h – Flow depth, b – Flume width, A- Cross-sectional Area of flow, P – Wetted perimeter, R – Hydraulic radius, V – Mean flow velocity, b/h – Aspect ratio | | | | | | | | |

It is observed from Table 4.1, that discharge is varied from $6.1314 \times 10^{-3}$ $m^3/s$ to $6.8149 \times 10^{-3}$ $m^3/s$ while keeping the slope constant at 0.004 in the first three runs. In the last two runs the different values of slope are considered while keeping the discharge constant at $6.4823\times 10^{-3}$ $m^3/s$. The mean velocity was found to vary from 0.311 m/s to 0.357 m/s while the mean flow depth was found to vary from 0.0604 m to 0.0687 m. For constant slope, with increase in discharge, flow depth increases and so does the velocity. When the discharge is kept constant and the slope is decreased, the flow depth increases while the velocity of flow is found to decrease.

Table 4.2 Hydrological and Geometrical parameters for flow with sunboard as bed form

| Q ($\times 10^{-3}$ $m^3/s$) | S | H (mm) | b (m) | A ($m^2$) | P (m) | R= A/P | V (cm/s) | b/h |
|---|---|---|---|---|---|---|---|---|
| 6.1314 | 4 | 47.5 | 0.305 | 0.01448 | 0.3999 | 0.0362 | 42.6 | 6.42 |
| 6.4823 | 4 | 48.5 | 0.305 | 0.01478 | 0.4019 | 0.0368 | 44.2 | 6.29 |
| 6.8149 | 4 | 49.6 | 0.305 | 0.01513 | 0.4042 | 0.0374 | 45.5 | 6.15 |
| 6.4823 | 6.7 | 46.9 | 0.305 | 0.01429 | 0.3987 | 0.0358 | 44.9 | 6.50 |
| 6.4823 | 2.86 | 51.5 | 0.305 | 0.01570 | 0.4079 | 0.0385 | 40.8 | 5.92 |
| Q – Discharge, S – Slope in mm/m, h – Flow depth, b – Flume width, A- Cross-sectional Area of flow, P – Wetted perimeter, R – Hydraulic radius, V – Mean flow velocity, b/h – Aspect ratio | | | | | | | | |

In these second five runs of experimental investigations, sunboard was fixed to the base of the channel section. Similar simulation of the flow parameters was performed and the results recorded. The results demonstrated the same trends as in the first five runs, in terms of flow

parameters. The flow velocity was increased and the flow depth decreased showing less resistance to the flow.

Table 4.3 Hydrological and Geometrical parameters for flow with Plastic fibre mat as the bed form.

| Q ($\times 10^{-3}$ $m^3/s$) | S | h (mm) | b (m) | A ($m^2$) | P (m) | R= A/P | V (cm/s) | b/h |
|---|---|---|---|---|---|---|---|---|
| 6.1314 | 4 | 93.2 | 0.305 | 0.02844 | 0.4915 | 0.0579 | 22.1 | 3.27 |
| 6.4823 | 4 | 93.8 | 0.305 | 0.02859 | 0.4925 | 0.0581 | 23.0 | 3.25 |
| 6.8149 | 4 | 94.3 | 0.305 | 0.02877 | 0.4936 | 0.0583 | 24.2 | 3.23 |
| 6.4823 | 6.7 | 87.4 | 0.305 | 0.02664 | 0.4797 | 0.0555 | 23.9 | 3.49 |
| 6.4823 | 2.86 | 103.4 | 0.305 | 0.03154 | 0.5118 | 0.0616 | 21.0 | 2.95 |
| Q – Discharge, S – Slope in mm/m, h – Flow depth, b – Flume width, A- Cross-sectional Area of flow, P – Wetted perimeter, R – Hydraulic radius, V – Mean flow velocity, b/h – Aspect ratio | | | | | | | | |

In these last five runs of experiments, a plastic fibre mat emulating small vegetation like pattern with its little vertical threads. Similar discharge slope variations were performed and the results noted. Similar trends were observed in terms of flow parameters although the flow velocity noted a significant drop while the flow depth increasing significantly which shows a greater resistance to flow than the above two cases.

### 4.3 Longitudinal velocity profiles for different materials

Longitudinal velocity readings were recorded using a pitot tube at three sections, 1m apart, in the flume channel section. Assuming x to be the distance of sections in the direction of flow, the three sections can be located at x = 3.15 m, 4.15 m and 5.15 m respectively. The observed velocity profiles are shown below.

#### 4.3.1 Longitudinal velocity profiles for Corroded Steel bed

Figures 4.1 and 4.2 show the longitudnal velocity distributions for simple channel with Corroded Steel bed for full flow depth at the three test sections.

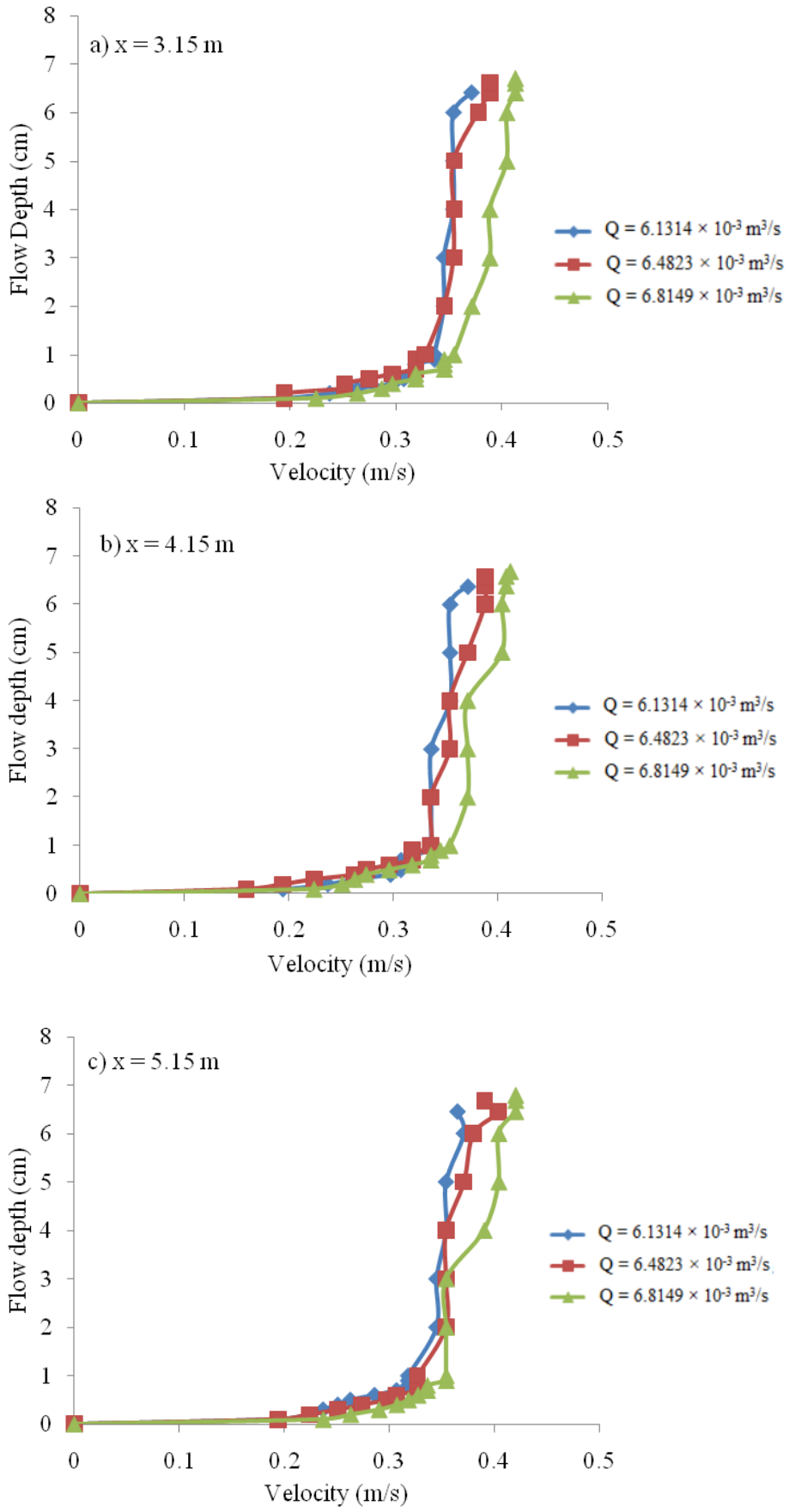


Figure 4.1 Longitudinal velocity profiles for Corroded Steel bed at a constant slope of 0.004 and varying discharges at a) x = 3.15 m, b) x = 4.15 m, and c) x = 5.15m

Figures 4.1(a-c) show the longitudinal velocity distribution for constant slope and with varying discharges. It is observed that the variation of longitudinal velocity distribution found to be small at three longitudinal channel sections i.e., x= 3.15 m, 4.15 m, and 5.15 m for a given discharge and slope while the velocity is seen to increase with an increase in discharge.

Figures 4.2 (a-c) show the longitudinal velocity distribution at various depths for constant discharge and with varying slopes. It is observed that the variation of vertical velocity distribution is comparatively small at three longitudinal channel sections i.e., x= 3.15 m, 4.15 m, and 5.15 m for a given discharge and slope while the velocity is seen to increase with an increase in slope.

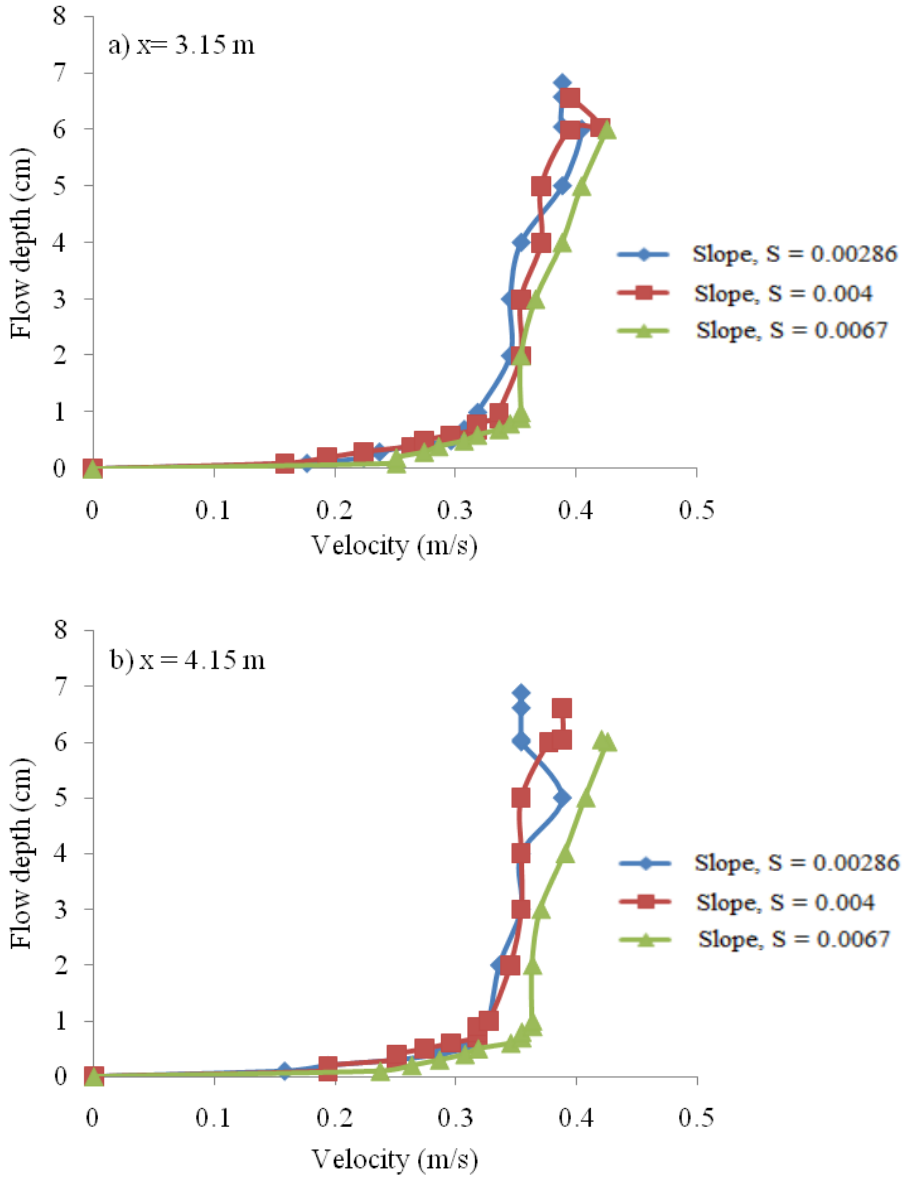

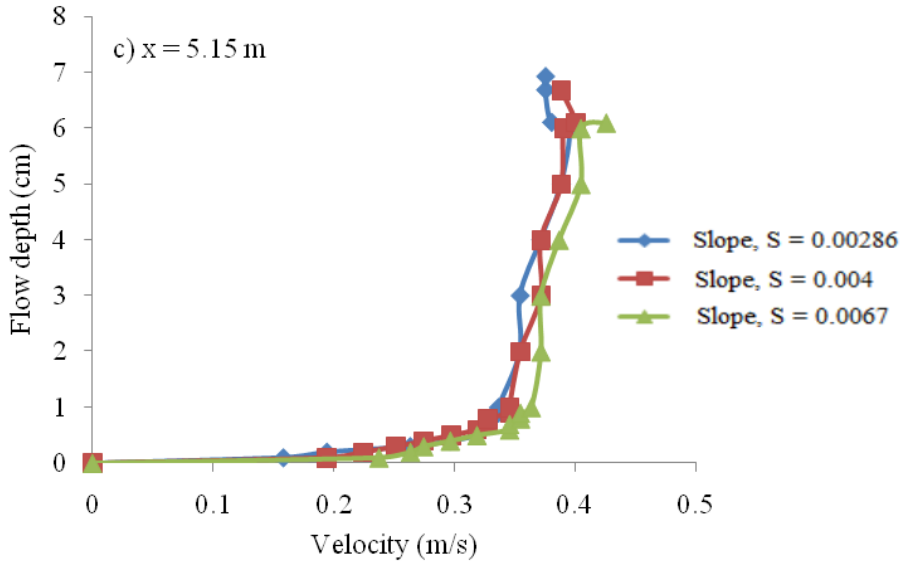


Figure 4.2 Longitudinal velocity profiles for corroded steel bed at a constant slope of $6.4823 \times 10^{-3}$ $m^3/s$ and varying slopes at a) x = 3.15 m, b) x = 4.15 m, and c) x = 5.15m

### 4.3.2 Longitudinal velocity profiles for sunboard

Figures 4.3 and 4.4 show the longitudinal velocity distributions for simple channel with Corroded Steel bed at the various flow depths.

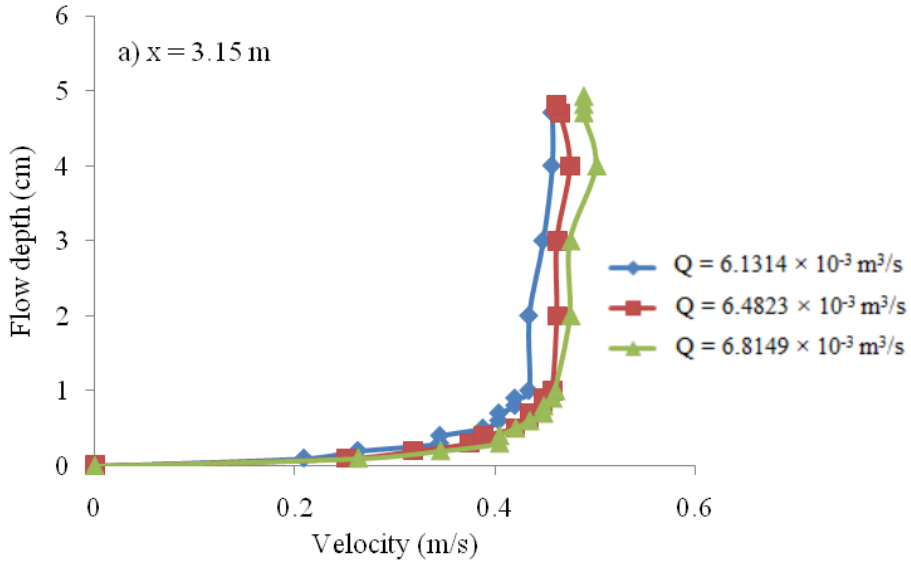

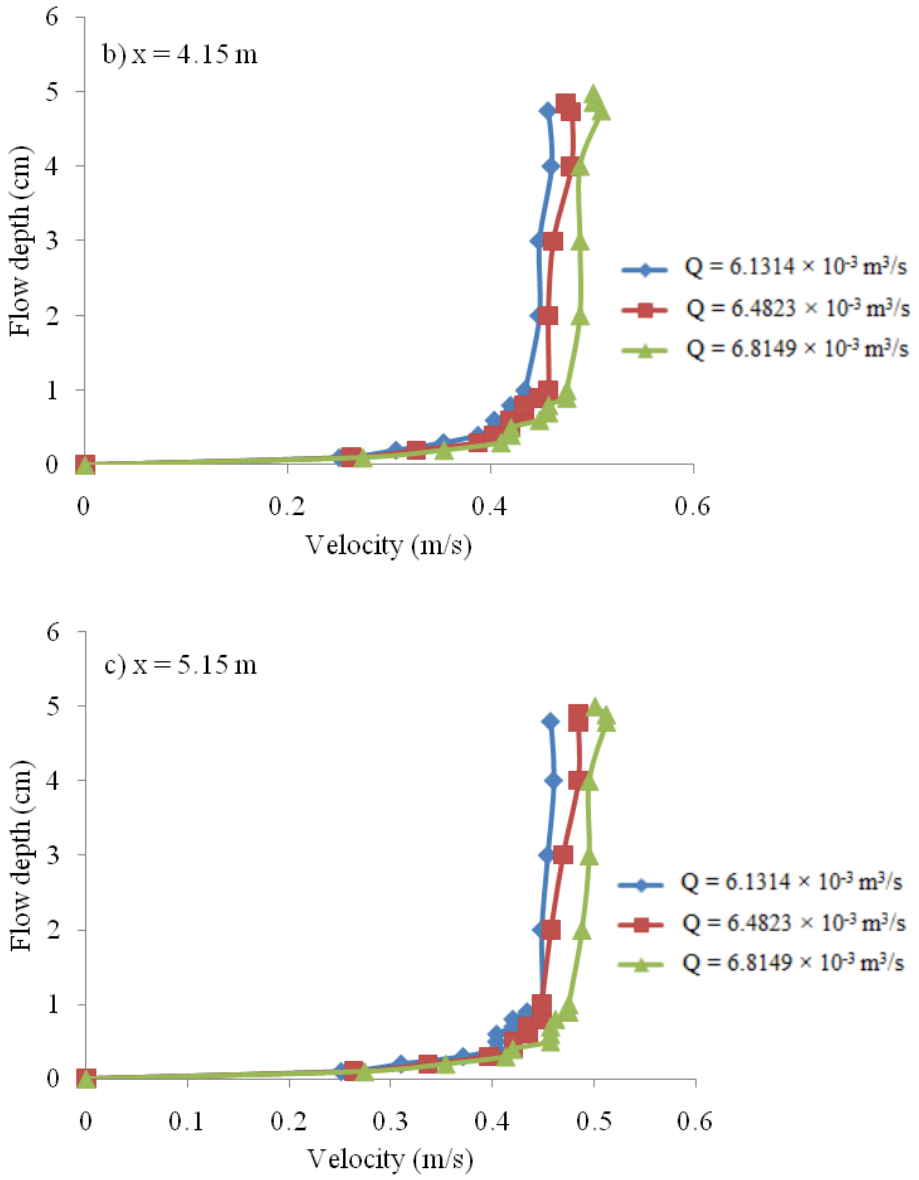


Figure 4.3 Longitudinal velocity profiles for sunboard at a constant slope of 0.004 and varying discharges at a) x = 3.15 m, b) x = 4.15 m, and c) x = 5.15m

Figures 4.3 (a-c) show the logitudinal velocity profiles for full depths at the three longitudinal sections in the flume for a constant slope of 0.004 and varying discharges. Generally, it can be observed that velocity tends to increase with an increase in the discharge, although it can be seen that the variation in velocity is small comparing to the variations observed in the case of corroded steel bed. This points to the fact that bed roughness has an impact on velocity distribution in a flow.

Figures 4.4 (a-c) show the longitudinal velocity distribution for sunboard for full depths at the three longitudinal test sections for a constant discharge of $6.4823 \times 10^{-3}$ $m^3/s$ and varying slopes. The increase in velocity with an increase in slope, though very small, can be observed. Due to being relatively smooth, sunboard offers less resistance to the flow.

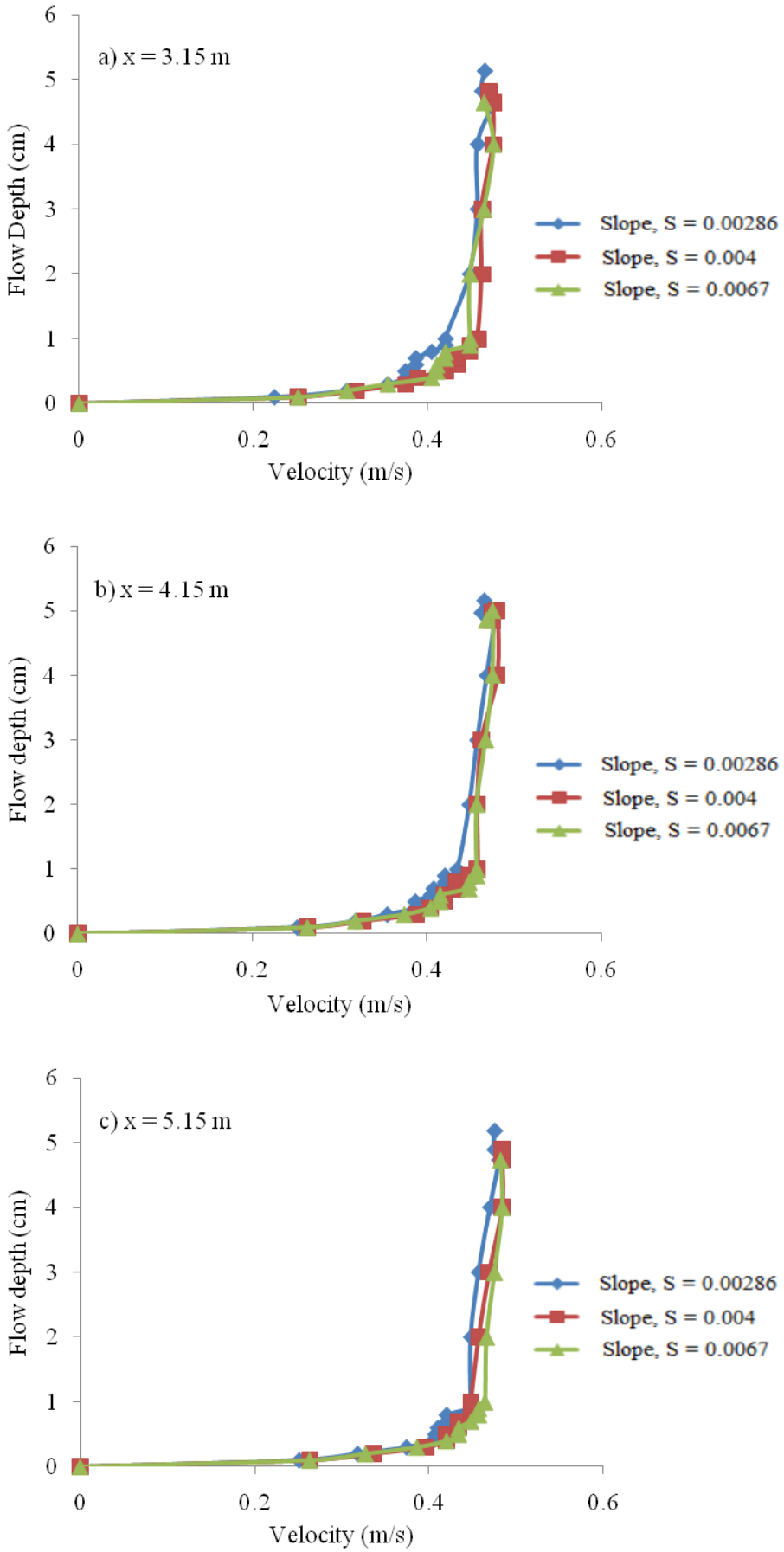


Figure 4.4 Longitudinal velocity profiles for sunboard at a constant discharge of $6.4823 \times 10^{-3}$ $m^3/s$ and varying slopes at a) x = 3.15 m, b) x = 4.15 m, and c) x = 5.15m

### 4.3.3 Longitudinal velocity profiles for plastic fibre mat

Figures 4.5 and 4.6 show the longitudinal velocity distribution for plastic fibre mat.

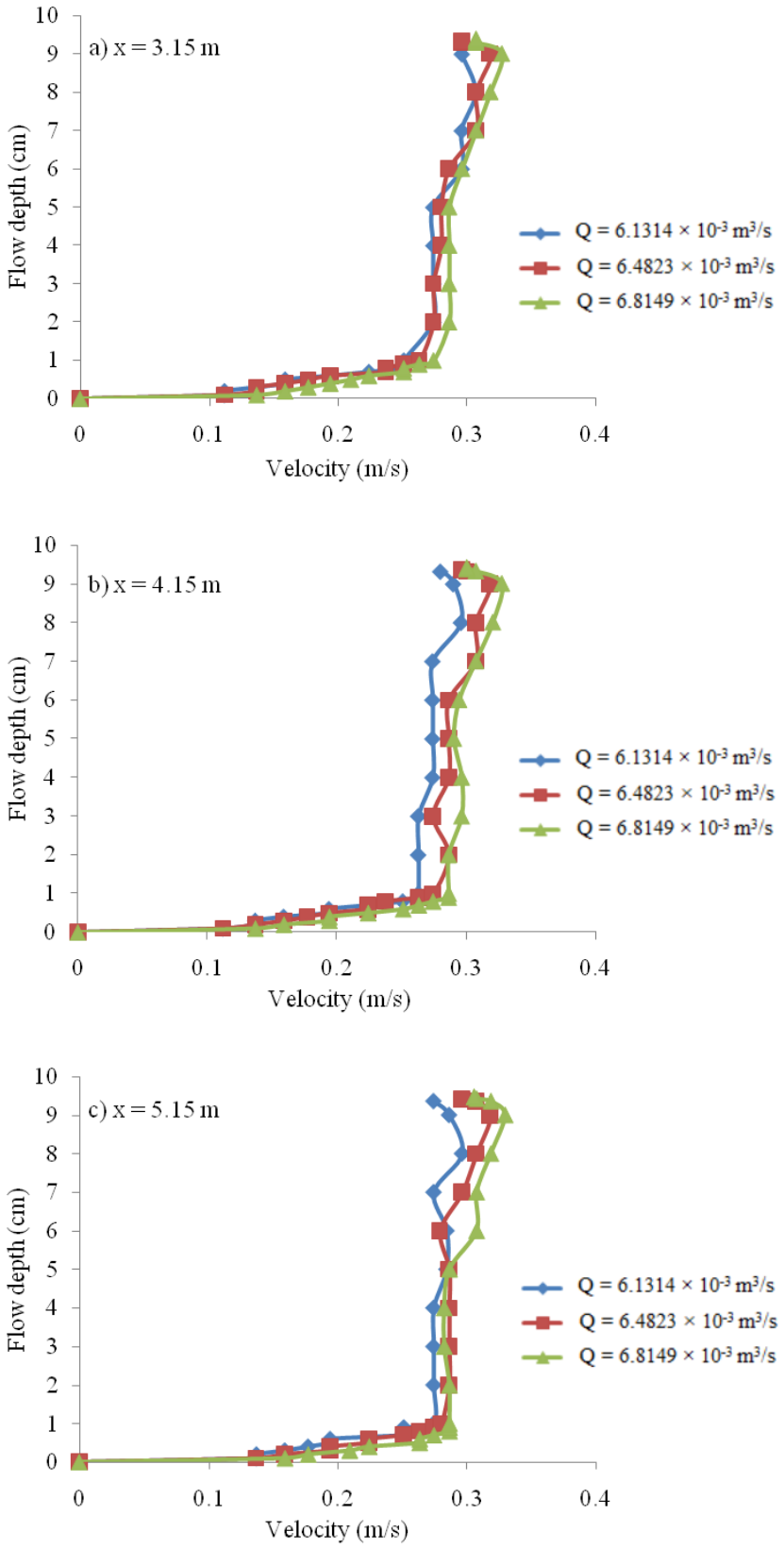


Figure 4.5 Longitudinal velocity profiles for plastic fibre mat at a constant slope of 0.004 and varying discharges at a) x = 3.15 m, b) x = 4.15 m, and c) x = 5.15m

Posing a higher roughness in comparison to the other two bed materials, the velocity profiles observed show considerable variations. Figs. 4.5 (a-c) show the distributions at the three longitudinal sections for a constant slope of 0.004 and varying discharges. The velocity distributions thus obtained indicate an increase in velocity with an increase in discharge. Velocity variation at the three sections are however small.

Figures 4.6 (a-c) show the longitudinal velocity distribution for Plastic fibre mat at the three longitudinal test sections for a constant discharge of $6.4823 \times 10^{-3}$ $m^3/s$ and varying slopes. It can be seen that velocity increases with an increase in slope. The changes in the velocity distributions are considerable at different test sections. This may be attributed to the roughness of mat.

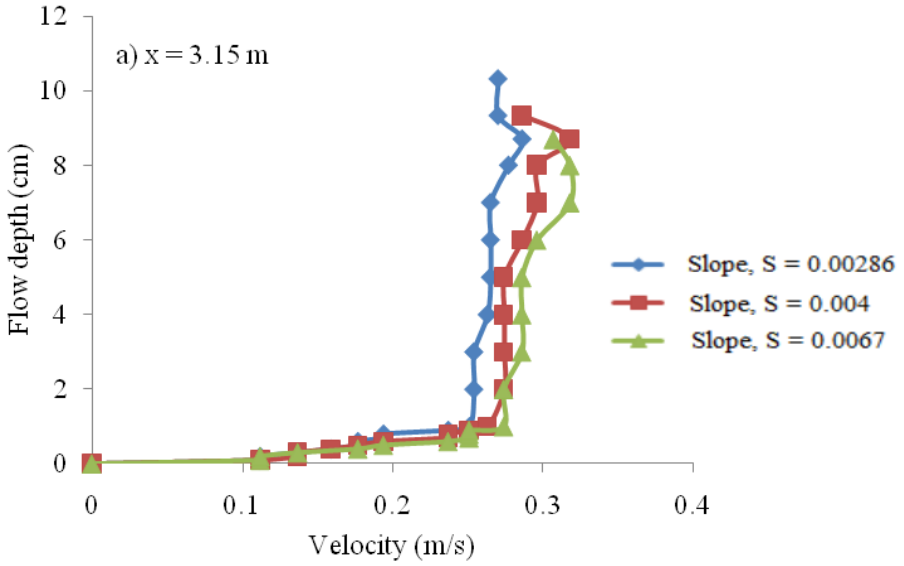


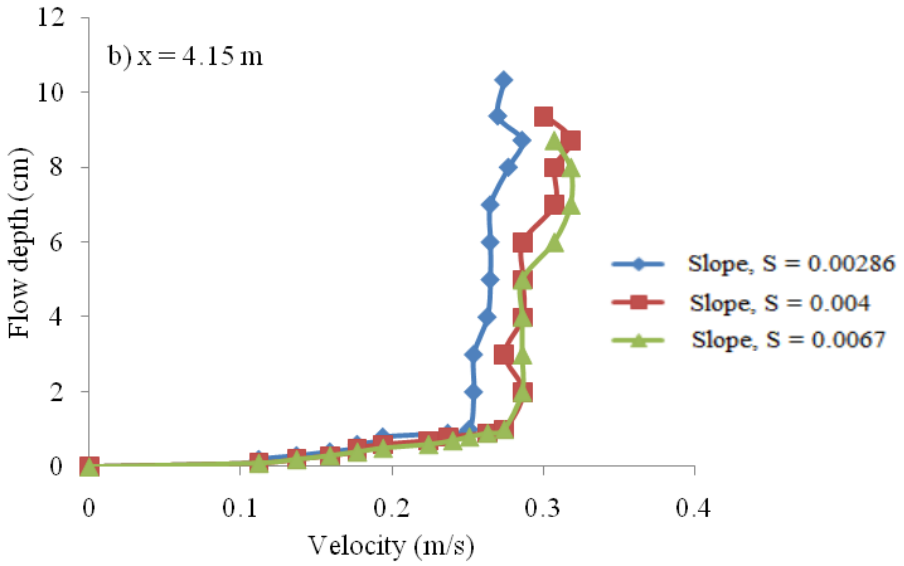

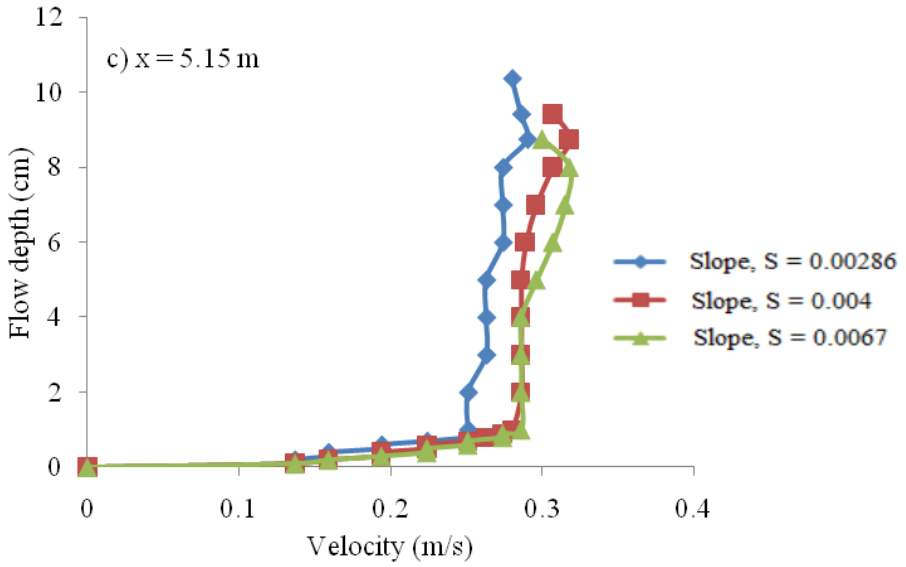


Figure 4.6 Longitudinal velocity profiles for Plastic fibre mat at a constant slope of 6.4823 × $10^{-3}$ $m^3$/s and varying slopes at a) x = 3.15 m, b) x = 4.15 m, and c) x = 5.15m

### 4.4 Roughness co-efficients

Tables 4.4, 4.5 and 4.6 tabulate the calculated values of various hydraulic parameters that affect or constitute the roughness in a channel. Tables 4.4, 4.5 and 4.6 also tabulate the calculated values of Manning's *n* and Chezy's *C* for Corroded Steel bed, sunboard and plastic fibre mat, respectively, for different flow conditions.

Table 4.4 Calculated values of *n* for Corroded Steel bed

| Q (× $10^{-3}$ $m^3$/s) | S | h (mm) | | | | V (cm/s) | b/h | *n* | *C* |
|---|---|---|---|---|---|---|---|---|---|
| | | $h_1$ | $h_2$ | $h_3$ | $h_{avg}$ | | | | |
| *Constant Slope, Variable Discharge* | | | | | | | | | |
| 6.1314 | 4 | 63.7 | 64.1 | 64.5 | 64.1 | 31.8 | 4.76 | 0.0256 | 23.310 |
| 6.4823 | 4 | 65.7 | 66.1 | 66.8 | 66.2 | 32.9 | 4.61 | 0.0253 | 23.615 |
| 6.8149 | 4 | 66.6 | 67.1 | 67.9 | 67.2 | 34.0 | 4.54 | 0.0247 | 24.32 |
| *Constant Discharge, Variable Slope* | | | | | | | | | |
| 6.4823 | 6.7 | 60.0 | 60.4 | 61.0 | 60.4 | 35.7 | 5.05 | 0.0287 | 20.534 |
| 6.4823 | 4 | 65.7 | 66.1 | 66.8 | 66.2 | 32.9 | 4.61 | 0.0253 | 23.615 |
| 6.4823 | 2.86 | 68.2 | 68.8 | 69.2 | 68.7 | 31.1 | 4.43 | 0.0226 | 26.597 |
| Q – discharge, S- Slope in mm/m, h- depth of flow, V- flow velocity, *n* – Manning's co-efficient and C- Chezy's co-efficient | | | | | | | | | |

Table 4.5 Calculated *n* values for sunboard as bed form

| Q ($\times 10^{-3}$ $m^3/s$) | S | h (mm) | | | | V (cm/s) | b/h | *n* | *C* |
|---|---|---|---|---|---|---|---|---|---|
| | | $h_1$ | $h_2$ | $h_3$ | $h_{avg}$ | | | | |
| *Constant Slope, Variable Discharge* | | | | | | | | | |
| 6.1314 | 4 | 47.1 | 47.4 | 47.9 | 47.5 | 42.6 | 6.42 | 0.0164 | 35.395 |
| 6.4823 | 4 | 48.2 | 48.5 | 48.9 | 48.5 | 44.2 | 6.29 | 0.0159 | 36.448 |
| 6.8149 | 4 | 49.3 | 49.7 | 50.0 | 49.6 | 45.5 | 6.15 | 0.0157 | 37.188 |
| *Constant Discharge, Variable Slope* | | | | | | | | | |
| 6.4823 | 6.7 | 46.5 | 46.8 | 47.3 | 46.9 | 44.9 | 6.50 | 0.0196 | 28.974 |
| 6.4823 | 4 | 48.2 | 48.5 | 48.9 | 48.5 | 44.2 | 6.29 | 0.0159 | 36.448 |
| 6.4823 | 2.86 | 51.3 | 51.6 | 51.8 | 51.5 | 40.8 | 5.92 | 0.0147 | 38.886 |
| Q – discharge, S- Slope in mm/m, h- depth of flow, V- flow velocity, *n* – Manning's co-efficient and C- Chezy's co-efficient | | | | | | | | | |

Table 4.6 Calculated *n* values for plastic fibre mat as bed form.

| Q ($\times 10^{-3}$ $m^3/s$) | S | h (mm) | | | | V (cm/s) | (b/h) | *n* | *C* |
|---|---|---|---|---|---|---|---|---|---|
| | | $h_1$ | $h_2$ | $h_3$ | $h_{avg}$ | | | | |
| *Constant Slope, Variable Discharge* | | | | | | | | | |
| 6.1314 | 4 | 92.9 | 93.2 | 93.6 | 93.2 | 22.1 | 3.27 | 0.0439 | 14.527 |
| 6.4823 | 4 | 93.3 | 93.7 | 94.2 | 93.8 | 23.0 | 3.25 | 0.0418 | 15.093 |
| 6.8149 | 4 | 93.8 | 94.1 | 94.5 | 94.3 | 24.2 | 3.23 | 0.0401 | 15.850 |
| *Constant Discharge, Variable Slope* | | | | | | | | | |
| 6.4823 | 6.7 | 0.0870 | 87.2 | 87.5 | 87.4 | 23.9 | 3.49 | 0.0489 | 12.389 |
| 6.4823 | 4 | 0.0933 | 93.7 | 94.2 | 93.8 | 23.0 | 3.25 | 0.0418 | 15.093 |
| 6.4823 | 2.86 | 0.1031 | 103.3 | 103.7 | 10.34 | 21.0 | 2.95 | 0.0406 | 15.818 |
| Q – discharge, S- Slope in mm/m, h- depth of flow, V- flow velocity, *n* – Manning's co-efficient and C- Chezy's co-efficient | | | | | | | | | |

The various calculated values of roughness parameters are evaluated and compared in the later sections of this chapter to understand the effect of roughness on steady flow conditions.

### 4.5 Variation of Manning's '*n*' with velocity for different bed forms

The calculated Manning's *n* were plotted against velocity readings for different bed materials to check and compare the observed trends as shown in Figs. 4.7 and 4.8 for constant slope and constant discharge respectively.

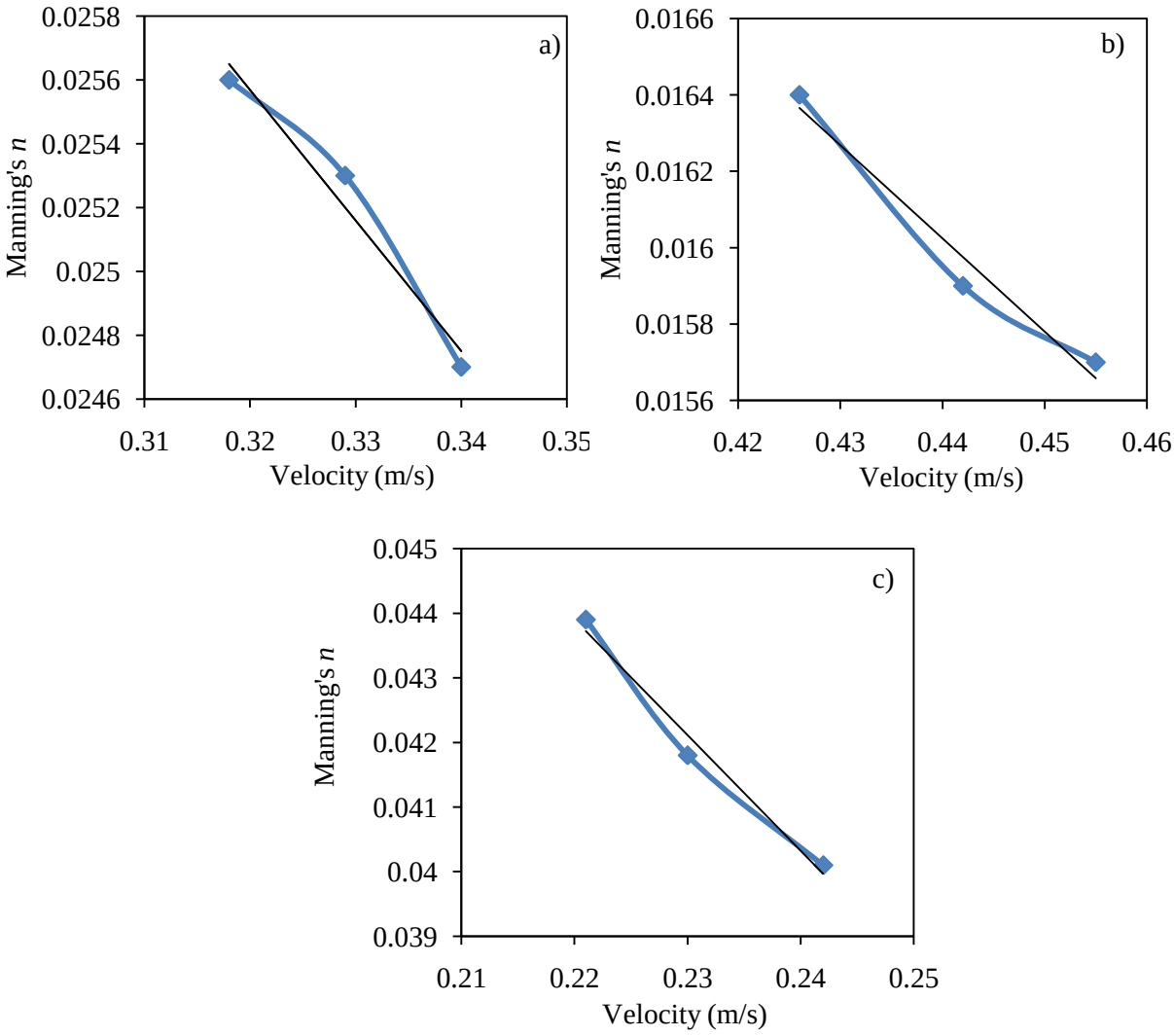


Figure 4.7 Variation of Manning's *n* with velocity at a constant slope of 0.004 and varying discharges for a) corroded steel bed, b) sunboard ,and c) plastic fibre mat

It can be seen from Fig 4.7 that for all the three materials, Manning's *n* tends to decrease with the increase in velocity. This shows that *n* is a function of velocity. Also, the *n* values calculated were lowest for sunboard and highest for plastic fibre mat. Similarly, for a constant discharge and increasing slope, *n* tends to increase with increase in slope for all bed materials, plastic fibre mat bearing the highest *n* value.

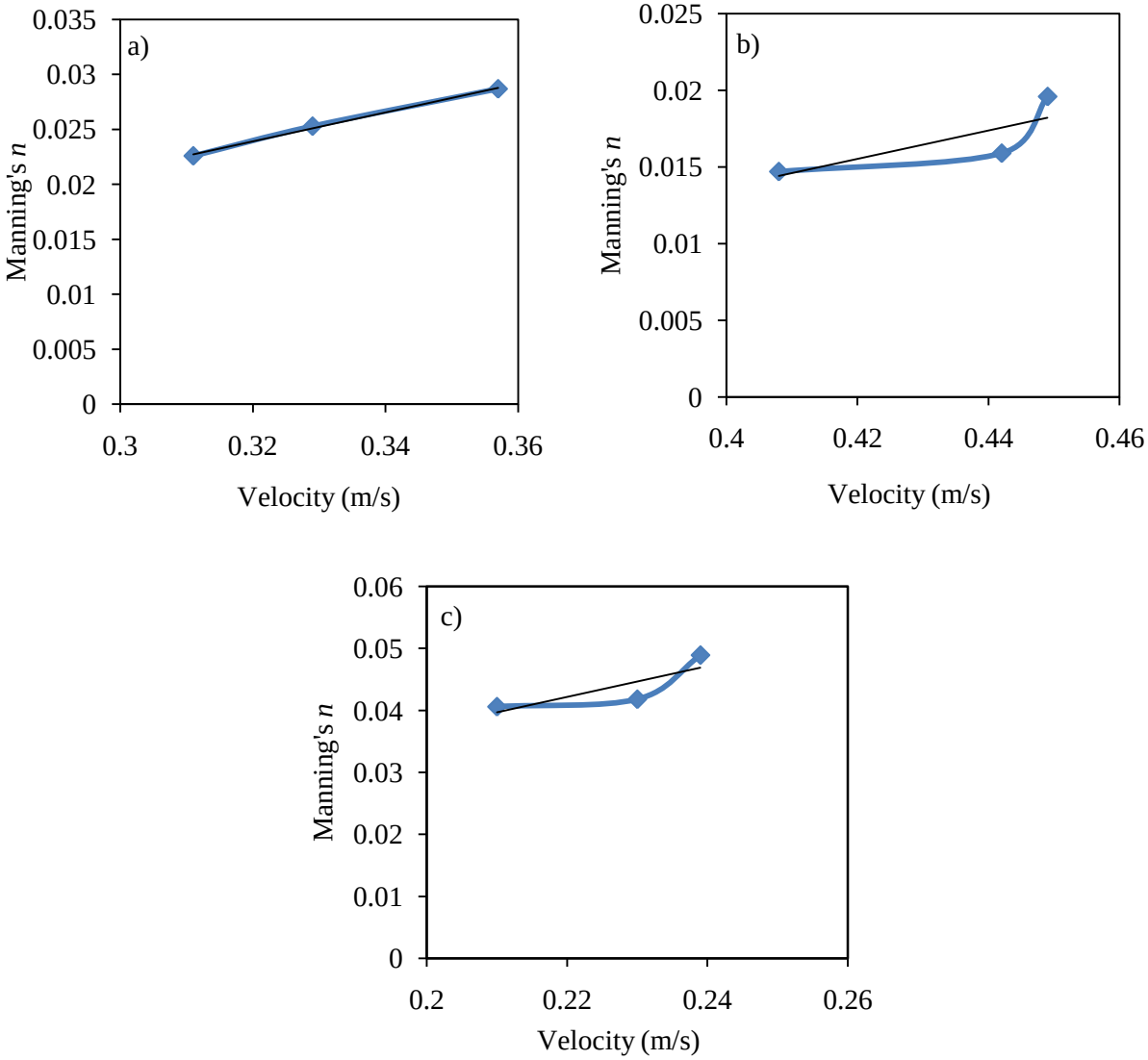


Figure 4.8 Variation of Manning's *n* with velocity at a constant discharge of $6.4823 \times 10^{-3}$ $m^3/s$ and varying slopes for a) corroded steel bed, b) sunboard ,and c) plastic fibre mat

### 4.6 Variation of Chezy's coefficient (*C*) with velocity for different bed forms

The values of Chezy's *C* were calculated for different bed materials under varying hydraulic conditions and were plotted against calculated velocity readings to observe the trends in its variation with varying flow parameters. The plots are shown in Figs. 4.9 and 4.10 for constant slope and constant discharge respectively.

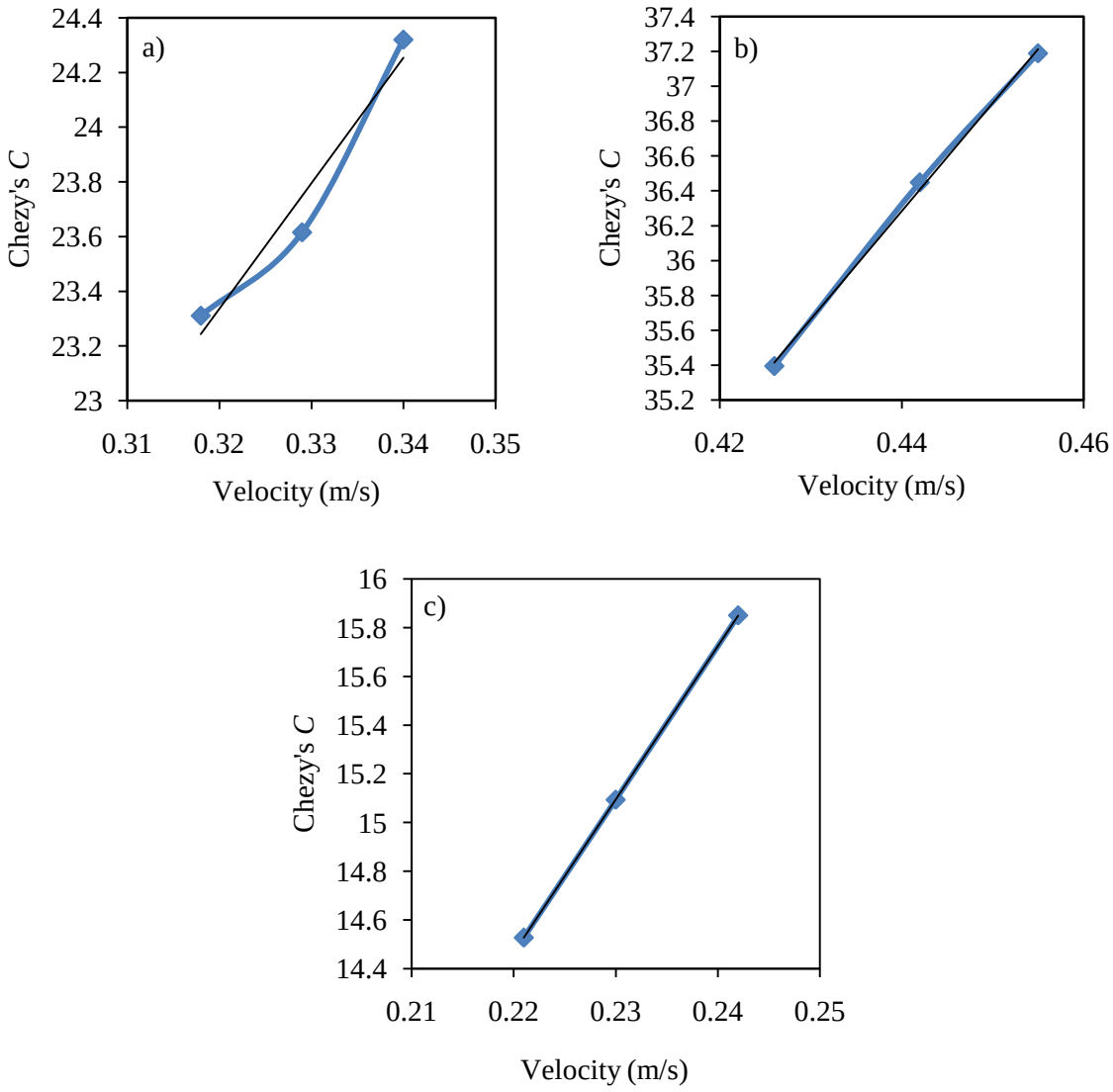


Figure 4.9 Variation of Chezy's *C* with velocity at a constant slope of 0.004 and varying discharges for a) Corroded Steel bed, b) sunboard ,and c) plastic fibre mat

We can see from Fig. (4.9) that for all the materials, the Chezy's co-efficient increases with an increase in velocity, for constant slope and varying discharges. It can also be observed that sunboard exhibited the highest values for Chezy's *C* while plastic fibre mat exhibited the lowest values. It can be seen that the material with highest *n* values had the lowest values of *C* and vice-versa. This verifies the the inversely proportional relationship between *n* and *C*. Variation of *C* with velocity for varying slopes under a constant discharge has been shown in Fig. (4.10).

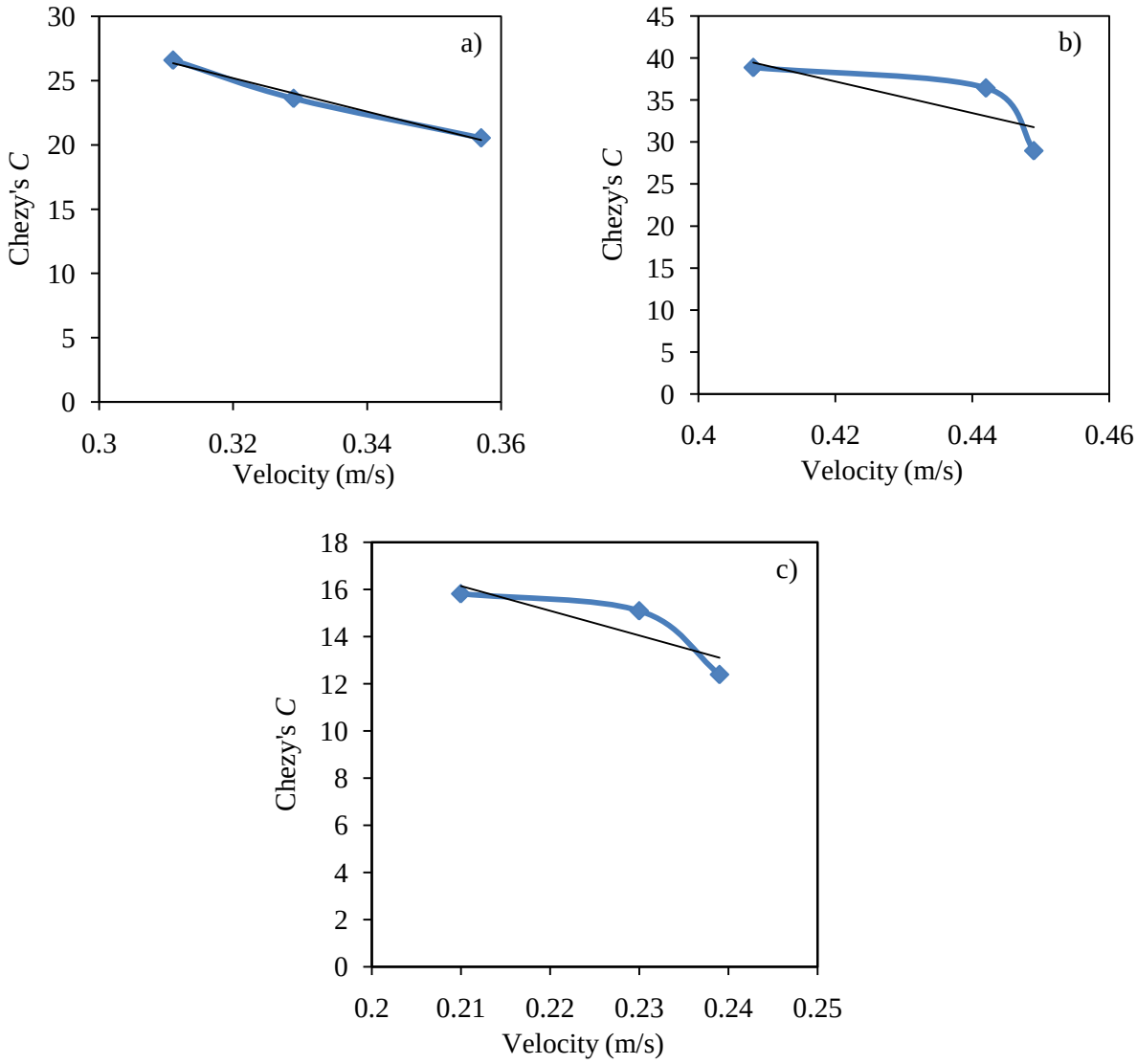


Figure 4.10 Variation of Chezy's *C* with velocity at a constant discharge of $6.4823 \times 10^{-3}$ $m^3/s$ and varying slopes for a) Corroded Steel bed, b) sunboard ,and c) plastic fibre mat

Similarly, for variable slope conditions and constant discharge, it can be seen from Fig. 4.10 that the value of Chezy's *C* decreases with increase in velocity.

### 4.7 Variation of *n* and *C* with aspect ratio for different bed forms

Aspect ratio is a geometrical parameter that has been used to estimate the roughness of channel. The width of the channel section of the flume was 0.305m. In the first five runs with no material at the base of flume, the depth varied from 0.0604 m to 0.06807 m and thus, the aspect ratio varied from 4.43 to 5.05.

In the second run of experiments with sunboard used as the bed base material, the depth varied from 0.0469 m to 0.0515 and hence the aspect ratio varied from 5.92 to 6.50. In the

third run of experiments with plastic fibre mat as the bed base material, the flow depth ranged from 0.0874 to 0.1034m and hence the aspect ratio was in the range of 2.95 to 3.49.

The variation of aspect ratio with *n* and *C* under different flow conditions has been shown in Fig. 4.11, 4.12, 4.13 and 4.14.

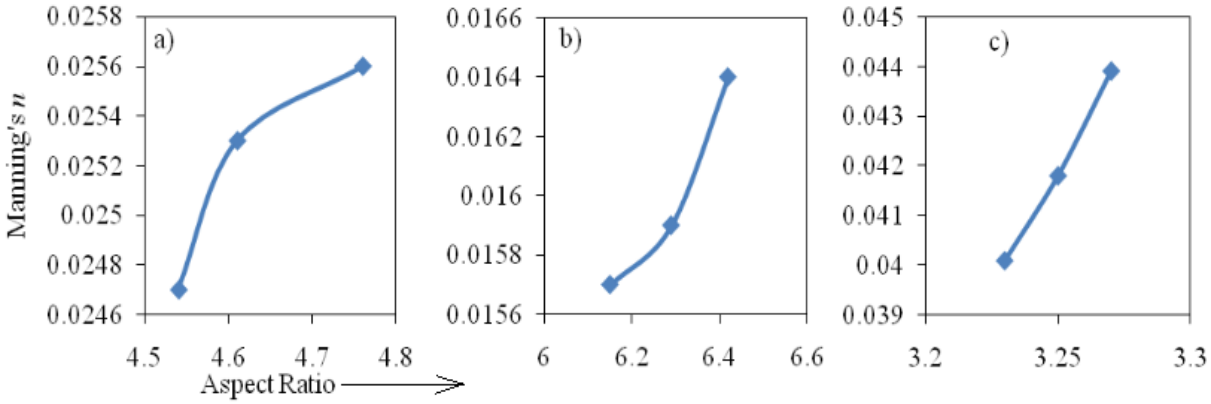


Figure 4.11 Variation of Manning's *n* with aspect ratio at a constant slope of 0.004 and varying discharges for a) Corroded Steel bed, b) sunboard ,and c) plastic fibre mat

It can be seen that *n* increases with an increase in the aspect ratio for all the given materials, keeping the slope constant and varying the discharge values.

Similarly, Fig. (4.12) shows that *n* tends to increase with the increase in aspect ratio. This shows that *n* increases with aspect ratio regardless of changes in flow conditions.

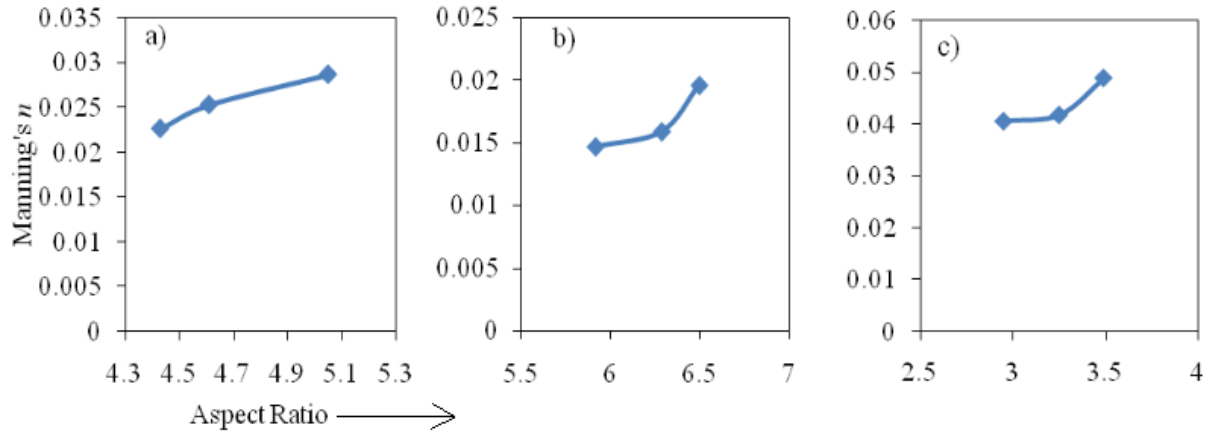


Figure 4.12 Variation of Manning's *n* with aspect ratio at a constant discharge of 6.4823 × $10^{-3}$ $m^3/s$ and varying slopes for a) Corroded Steel bed, b) sunboard ,and c) plastic fibre mat

The variation of *C* with aspect ratio has also been observed and shown in Fig. (4.13) below, for different flow conditions and materials.

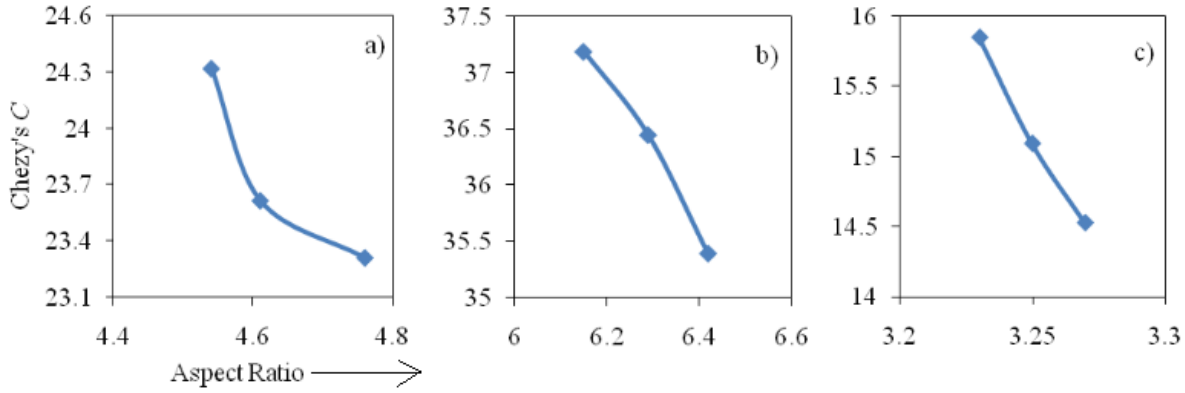


Figure 4.13 Variation of Chezy's *C* with aspect ratio at a constant slope of 0.004 and varying discharges for a) Corroded Steel bed, b) sunboard ,and c) plastic fibre mat

Fig. (4.13) shows that for a constant slope of 0.004 and variable discharges, Chezy's *C* decreases with an increase in the aspect ratio of the channel, for all the bed materials. Fig. (4.14) below shows a similar trend for a constant discharge of $6.4823 \times 10^{-3}$ $m^3/s$ and variable slopes. Hence it can be said that *C* decreases with an increase in aspect ratio regardless of flow conditions.

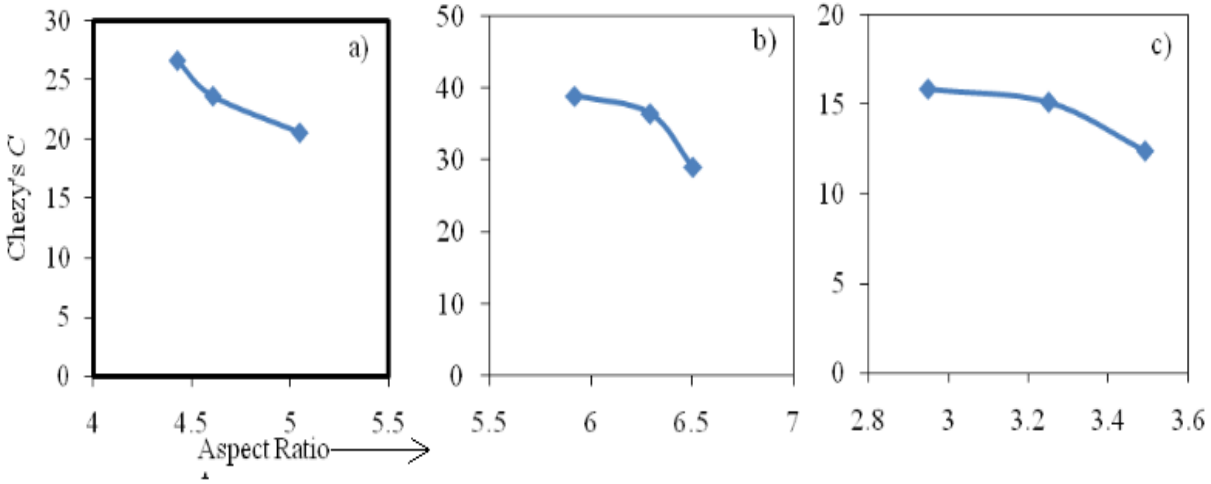


Figure 4.14 Variation of Chezy's *C* with aspect ratio at a constant discharge of $6.4823 \times 10^{-3}$ $m^3/s$ and varying slopes for a) Corroded Steel bed, b) sunboard ,and c) plastic fibre mat

### 4.8 Variation of Chezy's Coefficient (*C*) with Manning's Coefficient (*n*)

Fig. 4.15 and Fig. 4.16 illustrate the relationship between *n* and *C*. They clearly demonstrate the inverse relation between the two i.e., *n* increases with a decrease in *C* and vice-versa. It can also be seen that all the plots represent approximate straight lines verifying the relation between '*n*' and '*C*'.

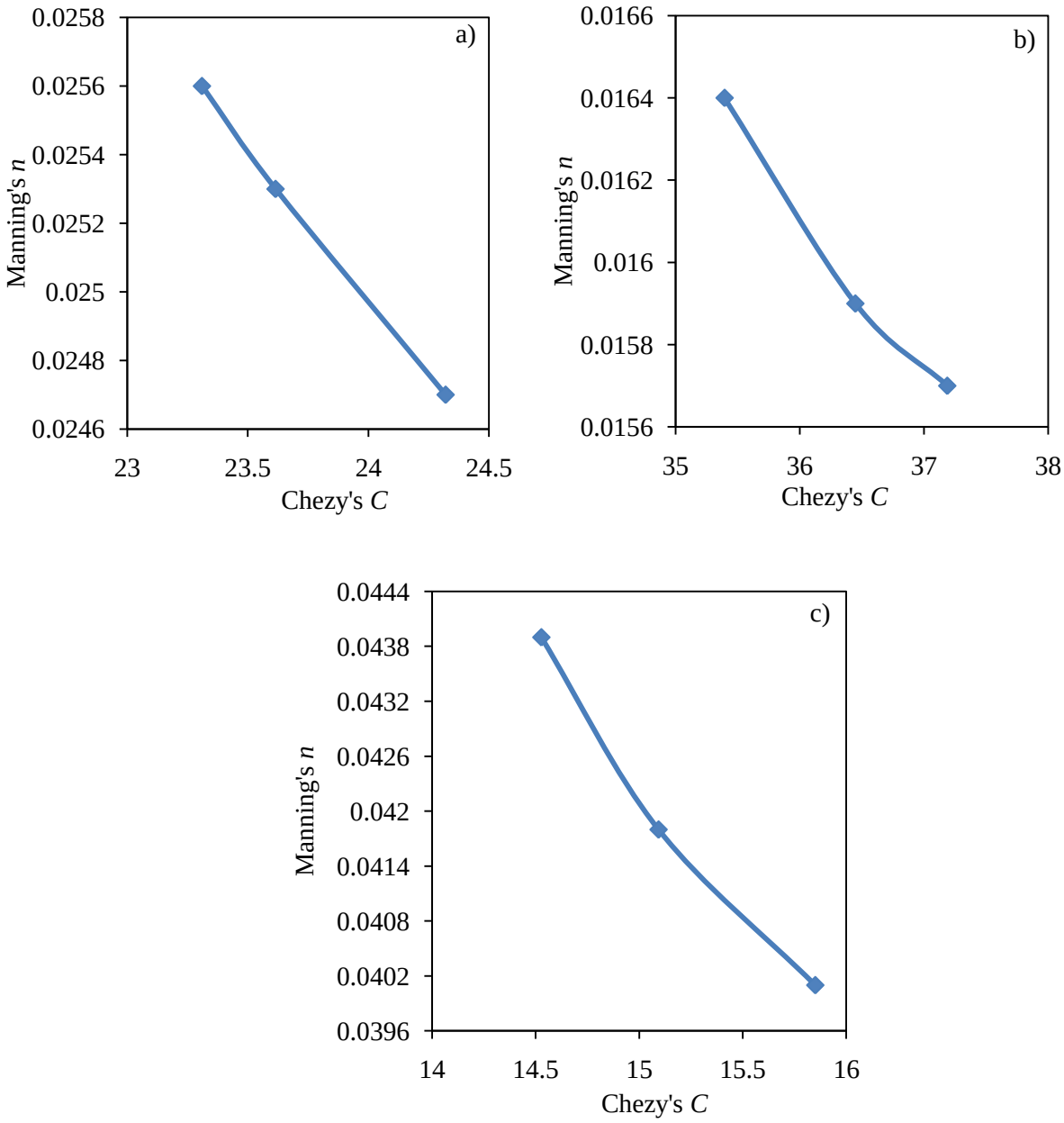


Figure 4.15 Variation of Manning's *n* with Chezy's *C* at a constant slope of 0.004 and varying discharges for a) Corroded Steel bed, b) sunboard ,and c) plastic fibre mat

Similar trends can be observed in Fig, 4.16, The curves are straight lines which shows that regardless of the hydraulic flow conditions, '*n*' and '*C*' share an inverse relation.

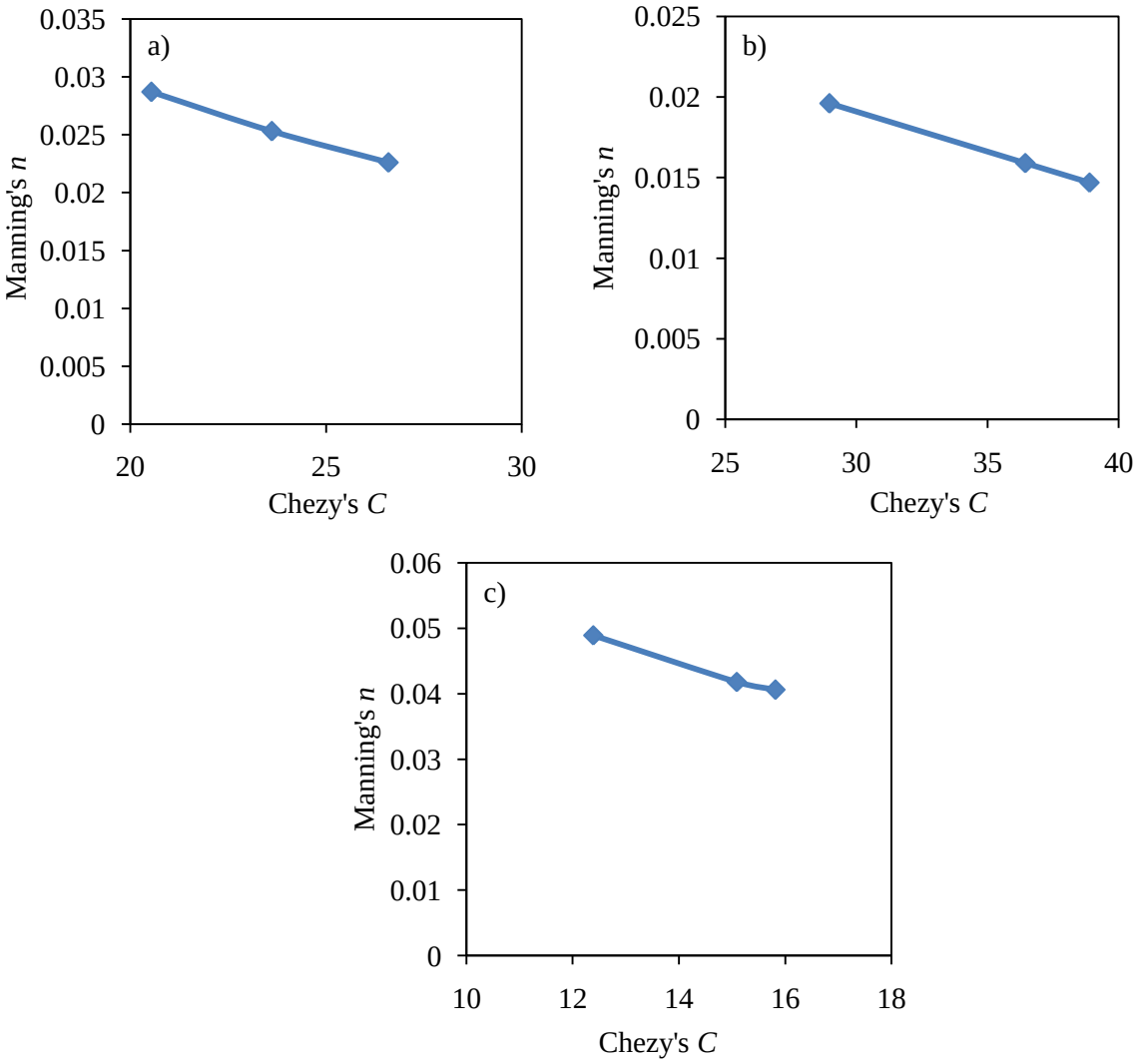


Figure 4.16 Variation of Manning's *n* with Chezy's *C* at a constant discharge of $6.4823 \times 10^{-3}$ $m^3/s$ and varying slopes for a) Corroded Steel bed, b) sunboard ,and c) plastic fibre mat

### 4.9 Roughness comparison between the various used bed materials

Figures 4.17 and 4.18 show the comparitive variation between roughness parameters of different bed materials that have been used.

Figure 4.17 (a) shows the variation between velocity and Manning's *n* at a constant slope and Fig. 4.17 (b) shows the variation between *n* and velocity at a constant discharge for different materials. Fig. 4.17 (a) shows that for a constant slope and increasing discharges, Manning's '*n*' decreases with an increase in velocity in a linear fashion. It can be observed that for no bed material, i.e., corroded steel bed the decrease in *n* is minimal compared to other bed materials.

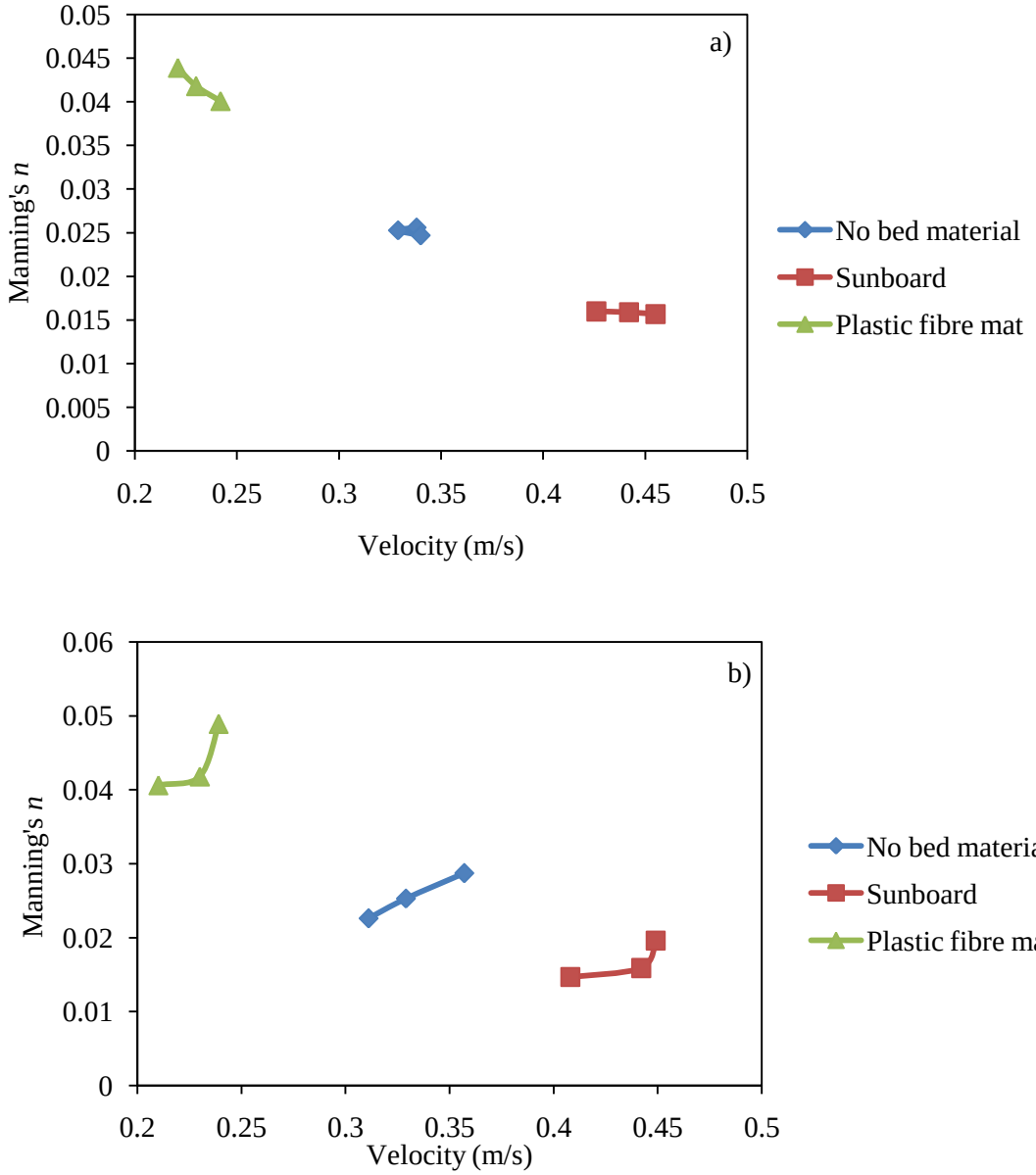


Figure 4.17 Comparison between *n* and velocity for all three materials (a) at constant slope (b) at constant discharge

Figure 4.17 (b) shows that for a constant discharge, Manning's '*n*' increases as the slope is increased. Corroded steel bed illustrates a linear fashion of increment while the other two bed materials show a sudden increase in the '*n*' values when the slope is increased from 0.004 to 0.0067.

Figure 4.18 (a) shows the variation between velocity and Chezy's *C* at a constant slope and Fig. 4.18 (b) shows the variation between *C* and velocity at a constant discharge for different materials. Fig. 4.18 (a) illustrates that for a constant slope, Chezy's *C* increases with an increase in discharge and velocity. It can be seen from Fig. 4.18 (a) that the increment exhibits a linear trend of increment.

Fig. 4.17 also shows that plastic fibre mat has the highest values of '*n*' while sunboard, being smoother compared to the other materials, has the lowest '*n*' values for all flow conditions.

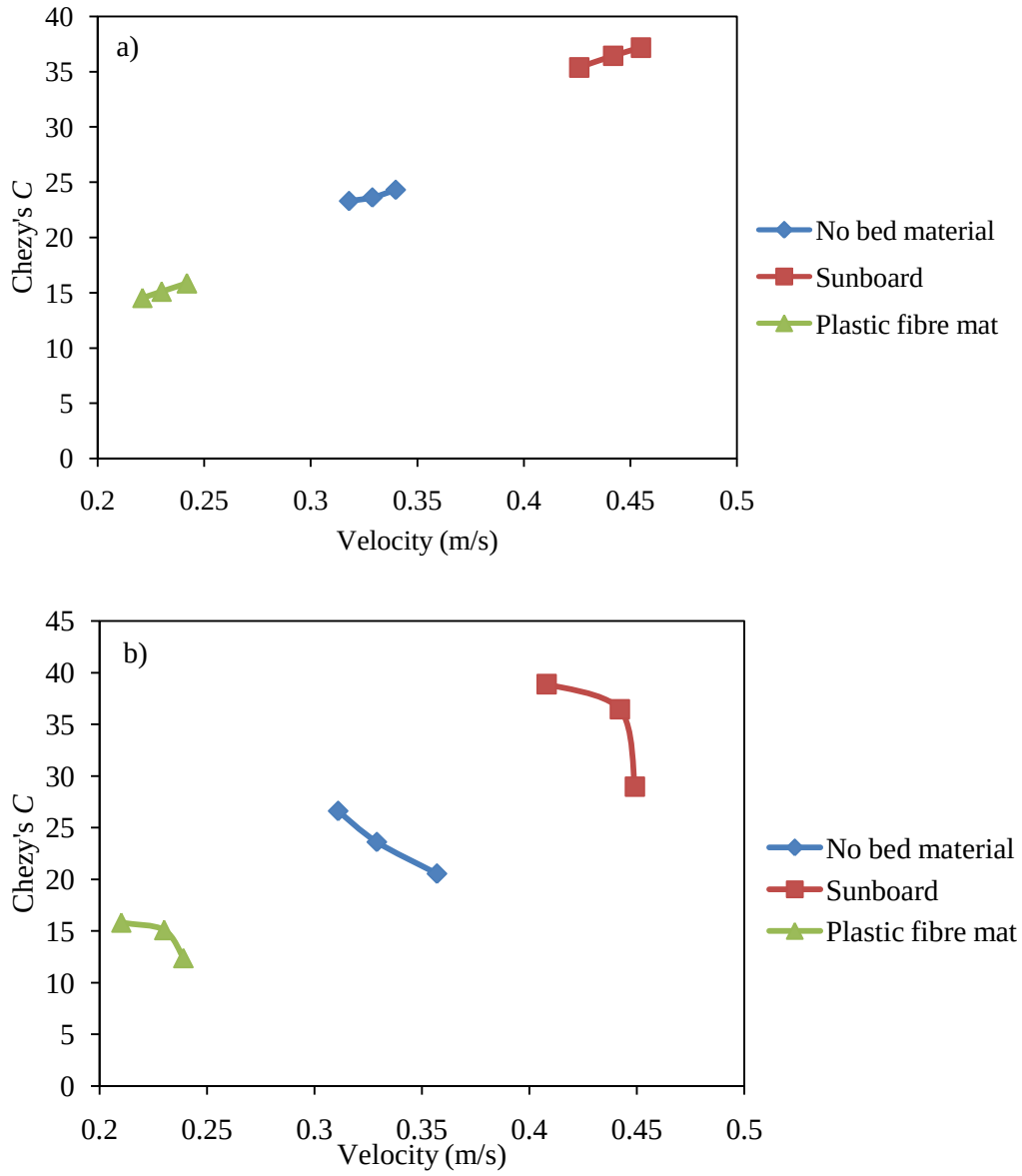


Figure 4.18 Comparison between *C* and velocity for all three materials (a) at constant slope (b) at constant discharge

It can also be observed from Fig. 4.18 (b) that at a constant discharge, Chezy's *C* decreases with an increment in slope and velocity. While the corroded steel bed shows a relatively linear trend of decrement, it can be seen that *C* values notice a sudden decrease when the slope value is changed from 0.004 to 0.0067. Fig. 4.18 also shows that plastic fibre mat has the lowest values of *C* while sunboard, being smoother compared to the other bed materials, has the highest *C* values for all flow conditions.

# CHAPTER 5

# CONCLUSIONS

All the experimental work was carried out at the Water resources laboratory of Thapar Institute of Engineering and Technology, Patiala. The experiments were performed for three types of bed condition. The first set of experiments was performed without fabricating the flume channel bed with any material while the second and third set of experiments were performed after fabricating the flume channel bed with two different materials, i.e., sunboard and plastic fibre mat. Every set of experiments included varying the discharge to three distinct values while keeping the slope constant and then varying the slopes, keeping the discharge, a constant. The major conclusions that can be drawn from the findings are-

- Velocity distribution for all materials follows a consistent trend of variation for a given flow condition. Velocity is found to vary consistently near the bed for all the materials used in the work but is fairly constant towards the surface.
- It can also be seen that the velocity variation for a flow condition is fairly minimal at the three different sections of the test reach. Of all the used bed materials, sunboard being the smoothest, shows the least amount of variations in the velocity trends while it can be seen that the highest velocity observations were made for sunboard as the bed material. Plastic fibre mat, on the other hand, exhibits a fair amount of variations in the velocity distribution trends.
- The values of Manning's *n* varied between 0.0226 and 0.0287 for corroded steel bed, between 0.0147 and 0.0196 for sunboard and between 0.0401 and 0.0489 for plastic fibre mat. The values of *n* were found to increase considerably with the decrease in slope for the case of varying slopes and constant discharge. While the *n* values decreased with an increase in discharge and flow depth, the variations were not as high in the case of flow with varying discharges and constant slope.
- The values of Chezy's *C* varied between 20.534 and 26.597 for corroded steel bed, between 28.974 and 38.886 for sunboard and between 12.389 and 15.850 for plastic fibre mat. It can thus be inferred that the material exhibiting the highest values of *n* i.e., plastic fibre mat is seen to have the lowest values of *C* and vice-versa.
- Manning's *n* is found to decrease with an increase in velocity for the case of constant slope while it increases with an increase in velocity for the case of constant discharge. The decrement for the case of constant slope was fairly linear while the *n* values took a sudden

leap of increment when the slope was increased from 0.004 to 0.0067. Manning's *n* also increased with an increase in aspect ratio for all the flow conditions.

- Chezy's *C* is found to increase with an increase in velocity for the case of constant slope while it decreases with an increase in velocity for the case of constant discharge. The increment for the case of constant slope was fairly linear while the *C* values took a sudden leap of decrement when the slope was increased from 0.004 to 0.0067. Chezy's *C* also decreased with an increase in aspect ratio for all the flow conditions.
- The variation between Manning's *n* values and Chezy's *C* was found to be inverse and fairly linear for all the flow conditions. Sunboard, among the three materials, was found to have the lowest roughness coefficient.

# FUTURE SCOPE OF WORK

The current work opens up a wide array of scope for the investigators to study the effects of bed roughness on the flow regime in an open channel flow. The data has been recorded for a limited data of discharge and slopes. Wide range of discharge and slope has not been considered due to time and capacity restraints. Future Investigators can attempt to study the role of bed roughness for a wide range of discharge and slope data in a compound channel cases. A model can be developed based on the experimental data and it can be simulated in natural open channels with varying regimes of flow. Roughness characteristics of bed vegetation can be studied in laboratory and natural channels. More accurate velocity data can be obtained and velocity distributions can be more extensively studied by using more accurate and sophisticated instruments like an Acoustic Doppler Velocimeter (ADV). Moreover the effect of side roughness and floodplains on flow needs to be studied. Variation of other resistance parameters like drag force due to vegetation and Darcy- Weisbach's friction factor, *f,* can be studied to gain a further insight into the role of roughness in flow regulation. Meanwhile, a whole range of bed materials can be selected and studied upon and work could also include non-prismatic, skewed and meandering channels.

# REFERENCES


1. Anwar, H. O. (1996). Velocity profile in shallow coastal waters. *Journal of Hydraulic Engineering*, 122(4), 220-223.
2. Cheng, N. S., & Chiew, Y. M. (1998). Modified logarithmic law for velocity distribution subjected to upward seepage. *Journal of Hydraulic Engineering*, 124(12), 1235-1241.
3. Chow, V. T. (1959). Open channel flow. *London: McGRAW-HILL*, 11(95), 99-136.
4. Cowan, W. L. (1956). Estimating hydraulic roughness coefficients. *Agricultural Engineering*, 37(7), 473-475.
5. Dalrymple, T., & Benson, M. A. (1967). Measurement of peak discharge by the slope-area method.
6. Dash, S. S., Khatua, K. K., & Mohanty, P. K. (2013). Factors influencing the prediction of resistance in a meandering channel. *CONTRIBUTORY PAPERS*, 303.
7. Fenzl, R. N., & Davis, J. R. (1964). Hydraulic resistance relationships for surface flows in vegetated channels. *Transactions of the ASAE*, 7(1), 46-0051.
8. Greco, M., Mirauda, D., & Plantamura, A. V. (2014). Manning's Roughness through the Entropy Parameter for Steady Open Channel Flows in Low Submergence. *Procedia Engineering*, 70, 773-780.
9. Huai, W. X., Zeng, Y. H., Xu, Z. G., & Yang, Z. H. (2009). Three-layer model for vertical velocity distribution in open channel flow with submerged rigid vegetation. *Advances in Water Resources*, 32(4), 487-492.
10. Ikeda, S., & Kanazawa, M. (1996). Three-dimensional organized vortices above flexible water plants. *Journal of Hydraulic Engineering*, 122(11), 634-640.
11. Kao, D. T., & Barfield, B. J. (1978). Prediction of flow hydraulics for vegetated channels. *Transactions of the ASAE*, 21(3), 489-0494.
12. Kouwen, N. N., & Li, R. M. (1980). Biomechanics of vegetative channel linings. *Journal of the Hydraulics Division*, 106(ASCE 15464).
13. Kouwen, N., Unny, T. E., & Hill, H. M. (1969). Flow retardance in vegetated channels. *Journal of the Irrigation and Drainage Division*, 95(2), 329-344.
14. Li, R. M., & Shen, H. W. (1973). Effect of tall vegetations on flow and sediment. *Journal of the hydraulics division*, 99(hy5).
15. Pang, B. (1998). River flood flow and its energy loss. *Journal of Hydraulic Engineering*, 124(2), 228-231.

16. Petryk, S., & Bosmajian III, G. (1975). Analysis of flow through vegetation. *Journal of the Hydraulics Division*, 101(ASCE# 114517 Proceeding).
17. Rhee, D. S., Ahn, H. K., Woo, H. S., & Kwon, B. (2007). Application and Assessment of New Vegetation Revetment Techniques Considering Safety against Flood and Environmental Performance. *Journal of Korea Water Resources Association*, 40(2), 125-134.
18. Righetti, M., & Armanini, A. (2002). Flow resistance in open channel flows with sparsely distributed bushes. *Journal of Hydrology*, 269(1-2), 55-64.
19. Sumer, B. M., Kozakiewicz, A., Fredsøe, J., & Deigaard, R. (1996). Velocity and concentration profiles in sheet-flow layer of movable bed. *Journal of Hydraulic Engineering*, 122(10), 549-558.
20. Saikia, M.D., & Das, M. (2016). Significance of different flow, channel and bed conditions in estimation of open channel flow resistance. *International Research Journal of Engineering and Technology*, 2(9), 856-860.
21. Temple, D. M. (1982). Flow retardance of submerged grass channel linings. *Transactions of the ASAE*, 25(5), 1300-1303.
22. Temple, D. M. (1986). Velocity distribution coefficients for grass-lined channels. *Journal of Hydraulic Engineering*, 112(3), 193-205.
23. Thompson, G. T., & Roberson, J. A. (1976). A theory of flow resistance for vegetated channels. *Transactions of the ASAE*, 19(2), 288-0293.
24. Wilkerson, G. V. (2007). Flow through trapezoidal and rectangular channels with rigid cylinders. *Journal of Hydraulic Engineering*, 133(5), 521-533.
25. Wu, F. C., Shen, H. W., & Chou, Y. J. (1999). Variation of roughness coefficients for unsubmerged and submerged vegetation. *Journal of hydraulic Engineering*, 125(9), 934-942.
26. Yang, K., Cao, S., & Knight, D. W. (2007). Flow patterns in compound channels with vegetated floodplains. *Journal of Hydraulic Engineering*, 133(2), 148-159.
27. Yang, K., Cao, S., & Liu, X. (2005). Study on resistance coefficient in compound channels. *Acta Mechanica Sinica*, 21(4), 353-361.

# DISSEMINATION OF WORK

- Goel, A. ,Das, B.S., & Babbar, R. (2018). “Roughness Coefficients variation in Simple Channel with Different Bed Materials ”, HYDRO-2019 INTERNATIONAL CONFERENCE (Hydraulics, Water Resources and Coastal Engineering). (Abstract submitted)

# Report

ORIGINALITY REPORT

| 16% | 11% | 7% | 8% |
|---|---|---|---|
| SIMILARITY INDEX | INTERNET SOURCES | PUBLICATIONS | STUDENT PAPERS |

PRIMARY SOURCES

| | | |
|---|---|---|
| 1 | ethesis.nitrkl.ac.in<br>Internet Source | 5% |
| 2 | Submitted to National Institute of Technology, Rourkela<br>Student Paper | 3% |
| 3 | digitalcommons.usu.edu<br>Internet Source | 1% |
| 4 | swat.tamu.edu<br>Internet Source | 1% |
| 5 | Taek-Kyung Lee. "Near-field diffraction pattern by an underground void of circular cylinder", Microwave and Optical Technology Letters, 05/1989<br>Publication | <1% |
| 6 | Wilkerson, Gregory V.. "Flow through Trapezoidal and Rectangular Channels with Rigid Cylinders", Journal of Hydraulic Engineering, 2007.<br>Publication | <1% |

| | | |
|---|---|---|
| 7 | Submitted to Thapar University, Patiala<br>Student Paper | <1% |
| 8 | www.arlis.org<br>Internet Source | <1% |
| 9 | Adrien, . "X-Y-Z", Computational Hydraulics and Hydrology An Illustrated Dictionary, 2003.<br>Publication | <1% |
| 10 | Submitted to South Bank University<br>Student Paper | <1% |
| 11 | Wu, Fu-Chun, Hsieh Wen Shen, and Yi-Ju Chou. "Variation of Roughness Coefficients for Unsubmerged and Submerged Vegetation", Journal of Hydraulic Engineering, 1999.<br>Publication | <1% |
| 12 | physicalplanning.ucsd.edu<br>Internet Source | <1% |
| 13 | Rajneesh Varma. "Effect of sparger design on hydrodynamics of a gas recirculation anaerobic bioreactor", Biotechnology and Bioengineering, 12/15/2007<br>Publication | <1% |
| 14 | www.clw.csiro.au<br>Internet Source | <1% |
| 15 | Romuald Szymkiewicz. "Open Channel Flow Equations", Water Science and Technology | <1% |

Library, 2010
Publication

| | | |
|---|---|---|
| 16 | www.mdpi.com<br>Internet Source | <1% |
| 17 | Subhasish Dey. "Fluvial Hydrodynamics", Springer Nature America, Inc, 2014<br>Publication | <1% |
| 18 | Submitted to University of Leeds<br>Student Paper | <1% |
| 19 | ueaeprints.uea.ac.uk<br>Internet Source | <1% |
| 20 | Donald W. Knight, Fenella A. Brown. "Resistance studies of overbank flow in rivers with sediment using the flood channel", Journal of Hydraulic Research, 2010<br>Publication | <1% |
| 21 | Submitted to Ecole Mondiale World School<br>Student Paper | <1% |
| 22 | ir.canterbury.ac.nz<br>Internet Source | <1% |
| 23 | Sundar Vallam, Murali Kantharaj, Noarayanan Lakshm. "Chapter 8 Resistance of Flexible Emergent Vegetation and Their Effects on the Forces and Runup Due to Waves", InTech, 2011<br>Publication | <1% |

| | | |
|---|---|---|
| 24 | shlagbaum-surgut.ru<br>Internet Source | <1% |
| 25 | hal.archives-ouvertes.fr<br>Internet Source | <1% |
| 26 | eprints.utm.my<br>Internet Source | <1% |
| 27 | Submitted to University of Greenwich<br>Student Paper | <1% |
| 28 | Submitted to University Tun Hussein Onn Malaysia<br>Student Paper | <1% |
| 29 | Submitted to Rochester Institute of Technology<br>Student Paper | <1% |
| 30 | Miroslaw Narbutt, Mark Davis. "The capability of the EDCA mechanism to support voice traffic in a mixed voice/data transmission over 802.11e WLANs - an experimental investigation", 32nd IEEE Conference on Local Computer Networks (LCN 2007), 2007<br>Publication | <1% |
| 31 | Fengpeng Bai, Zhonghua Yang, Wenxin Huai, Chuandong Zheng. "A Depth-averaged Two Dimensional Shallow Water Model to Simulate Flow-rigid Vegetation Interactions", Procedia Engineering, 2016<br>Publication | <1% |

| | | |
|---|---|---|
| 32 | Huai, W.X.. "Three-layer model for vertical velocity distribution in open channel flow with submerged rigid vegetation", Advances in Water Resources, 200904<br>Publication | <1% |
| 33 | eprints.worc.ac.uk<br>Internet Source | <1% |
| 34 | sheetalflex.com<br>Internet Source | <1% |
| 35 | www.citeulike.org<br>Internet Source | <1% |
| 36 | Submitted to University of Bradford<br>Student Paper | <1% |
| 37 | Dong Sop Rhee. "Hydraulic resistance of some selected vegetation in open channel Flows", River Research and Applications, 06/2008<br>Publication | <1% |
| 38 | Submitted to iGroup<br>Student Paper | <1% |
| 39 | www.jofamericanscience.org<br>Internet Source | <1% |
| 40 | download.e-pubs.nl<br>Internet Source | <1% |
| 41 | Depeweg, . "Open Channel Flow", UNESCO- | |

| | | |
|---|---|---|
| | IHE Delft Lecture Note Series, 2006.<br>Publication | <1% |
| 42 | www.itc.nl<br>Internet Source | <1% |
| 43 | vuir.vu.edu.au<br>Internet Source | <1% |
| 44 | Ercan, Ali, M. Levent Kavvas, and Ismail Haltas. "Scaling and self-similarity in one-dimensional unsteady open channel flow", Hydrological Processes, 2013.<br>Publication | <1% |
| 45 | dspace.brunel.ac.uk<br>Internet Source | <1% |
| 46 | docs.di.fc.ul.pt<br>Internet Source | <1% |
| 47 | tel.archives-ouvertes.fr<br>Internet Source | <1% |
| 48 | uos-app00353-si.soton.ac.uk<br>Internet Source | <1% |
| 49 | mafiadoc.com<br>Internet Source | <1% |
| 50 | S. T. Lin. "MODIFIED WATER QUANTITY RECEIVING MODEL FOR FLORIDA CONSERVATION AREAS", Journal of the | <1% |

American Water Resources Association, 2/1979
Publication

---

51 Cheng, Nian-Sheng, Hoai Thanh Nguyen, Soon Keat Tan, and Songdong Shao. "Scaling of Velocity Profiles for Depth-Limited Open Channel Flows over Simulated Rigid Vegetation", Journal of Hydraulic Engineering, 2012. <1%
Publication

---

52 M.A. Mammadova. "DEMANDS ON, CONDITION, AND ENVIRONMENTAL PROBLEMS OF THE BAKUMUNICIPAL WATER SUPPLY", NATO Science Series, 2006 <1%
Publication

---

53 S. Banerjee, B. Naik, P. Singh, K. K. Khatua. "Flow resistance in gravel bed open channel flows case: intense transport condition", ISH Journal of Hydraulic Engineering, 2018 <1%
Publication

---

| | | | |
|---|---|---|---|
| Exclude quotes | Off | Exclude matches | Off |
| Exclude bibliography | Off | | |